INTERNATIONAL JOURNAL OF INNOVATIVE RESEARCH & DEVELOPMENT

ISSN 2278 – 0211 (Online)

# Enhancing the Performance and Life Cycle of Lithium –Sulfur Batteries by Nanostructured Carbon and Different Additives

**A.M.El Shafey**
Assistant Professor, Department, of Physical Chemistry, King Khaled University, Saudi Arabia

***Abstract:***
*Lithium sulfur (Li – S) battery has been considered as one of the most promising rechargeable batteries among various energy storage devices owing to their low cost, high specific capacity and energy density. Over the last decade, lithium sulfur (Li – S) batteries have been extensively studied because of the abundance of sulfur, their environmental benignity, and high gravimetric (2600 Wh $Kg^{-1}$) and (2800 Wh $L^{-1}$) energy densities and are promising candidates for meeting future-energy storage demands. However, the insulation of sulfur and high solubility of lithium polysulfides, swelling of cathode value and formation of lithium dendrites results in the low utilization and poor cycling performance. Significant efforts have been made to trap polysulfides via physical strategies using carbon based materials, but interactions between polysulfides and carbon are so weak that the device performance is limited. Chemical strategies provide the relatively complemented routes for improving the batteries' electrochemical properties by introducing strong interactions between functional groups and (oxygen, nitrogen and boron, etc.) and chemical additives (metal, polymers, etc.) to the carbon structure and how these foreign guests immobilize the dissolved polysulfide. This review focused on recent studies have reported various material such as metal oxides and sulfides that interact strongly with polysulfides species and can alleviate the dissolution problem by comparing the polysulfides adsorption capability candidate materials to provide the useful strategy to screen for suitable candidate materials and valuable information for rational design. Overcoming the loss of active mass and stabilizing cell capacity at high rates is pivotal to the realization of practical Li-S cells. In this review, different separate concepts and materials were studied with the aim to improve the Li-S batteries capacity, cycle life and capacity retention.*

***Keywords****: Lithium-sulfur batteries, Additives, Shuttle effect, Polysulfides, Life cycle, Performance; discharge, advanced cathode materials; carbon nanotube*

## 1. Introduction

The ever-increasing environment pollution and the decreasing fossil fuels force people to develop renewable energy, and it is wise to store and release the spare energy in certain forms whenever needed. Thus, the highly efficientenergy storage system has attracted extensive interest in recenty ears, and various applications have been found in mobiledevices, electric vehicles, and sustainable energy industry. Dueto their light weight, high open circuit voltage, high capacity,and non-memory effect, lithium-ion batteries have been commercialized since 1990s by Sony corporation and dominated the market for portable electronic devices [1] .

With the increase in energy consumption and change of global climate, a sustainable, low-cost and environmentally friendly electrical energy storage systems with high energy densities should be considered necessarily [1–5].If electric vehicles (EVs) replace the majority of gasoline powered transportation, Li-ion batteries will significantly reduce greenhouse gas emissions [6]. Thus, the highly efficient energy storage system has attracted extensive interest in recent years, and various applications have been found in mobile devices, electric vehicles, and sustainable energy industry. Due to their light weight, high open circuit voltage, high capacity, and non-memory effect. Li-ion batteries have an unmatchable combination of high energy and power density, making it the technology of choice for portable electronics, power tools, and hybrid/full electric vehicles [7]. The high energy efficiency of Li ion batteries may also allow their use in various electric grid applications, including improving the quality of energy harvested from wind, solar, geo-thermal and other renewable sources, thus contributing to their more widespread use and building an energy-sustainable economy. Therefore Li-ion batteries are of intense interest from both industry and government funding agencies, and research in this field has abounded in the recent years. Firstly, Li has the lowest reduction potential of any element, allowing Li based batteries to have the highest possible cell potential. Also, Li is the third lightest element and has one of the smallest ionic radii of any single charged ion. These factors allow Li-based batteries to have high gravimetric and volumetric capacity and power density. Finally, although multivalent cations allow for higher charge capacity per ion, the additional charge significantly reduces their mobility. Given that ionic diffusion in the solid electrodes is often the rate-limiting factor for battery power performance, this presents an enormous hurdle for the development of such alternative chemistries.Lithium-sulfur batteries (LSBs) are competitive and promising choice, which has higher theoretical specific capacity of 1675 mAh $g^{-1}$ and theoretical energy density of 2600 Wh $kg^{-1}$ compared to commercialized lithium-ion batteries[8–14]. Particularly, a crucial characteristic of LSBs is that $S_8$ molecules can bind two Li

atoms per S atom [$S_8$+ 16Li8$Li_2S$][15–18].Thus, compared to other cathode materials, the energy density and electrochemical performance of sulfur electrode can be significantly improved[19]. In addition, sulfur is one of the basic elements of the earth, and it is obtained extensively from nature. Moreover, sulfur is abundantand possessing great superiority compared with the limited and pollution-yielding fuel oil.Sulfur is cheap and non-toxic[20–23]. The attempt of utilizing sulfur element as electrode material was first made in 1962 by Herbet and Ulam [24]. The conventional LSBs are composed of sulfur cathode, lithium anode, and organic liquid electrolyte [25–27]. In LSBs, the discharge process of sulfur cathode includes three main steps: Firstly, solid to solution reduction of $S_8$ molecule into long-chain poly sulfides; Secondly, solution phase reduction of long-chain polysulfides into short-chain polysulfides; Finally, solution to solid reduction of the short-chain polysulfides into insulating and insoluble $Li_2S_2$ and $Li_2S$[19]. The amount of Li available on the Earth's crust is sufficient to power a global fleet of automobiles [28]. Rising prices though, can be problematic for LSBs batteries because cost is the major factor inhibiting its expansion into renewable energy applications. Even so, Li is not a major factor in the cost of LSBs batteries at present. Li is used in the cathode and electrolyte, which make up only a small portion ofthe overall cost [29]. Within these components the cost of processing and the cost of cobalt in cathodes are the major contributing factors [30]. Given its fundamental advantages, Li-ion sulfur batteries will in all likelihood continue to dominate portable electrochemical energy storage for many years to come. Since Li-ion sulfur batteries are the second choice source of portable electrochemical energy storage, improving their cost and performance can greatly expand their applications and enable new technologies which depend on energy storage. A great volume of research in Li-ion sulfur batteries has thus far been in electrode materials. Electrodes with higher rate capability, higher charge capacity, and (for cathodes) sufficiently high voltage can improve the energy and power densities of Li batteries and make them smaller and cheaper. However, this is only true assuming that the material itself is not too expensive or rare. Figure 1a shows the wholesale price of various metals and the abundance of elements as a fraction of the Earth's crust [31]. Although the electrodes are not fabricated from pure metal ingots, the prices illustrate the relative differences. Mn is clearly much cheaper than Co, explaining the cost difference in the cathode materials made from these two metals. The abundance of elements represents a limitation on the availability of the element. While true availability also depends on supply and demand, this chart shows advantages of some elements. For example, P and S are much more abundant than the more conductive elements in Groups V and VI, respectively. Finally, the theoretical specific and volumetric capacities of the elements which undergo conversion reactions with Li are shown in Fig. 1b. Unfortunately, as useful as the periodic table is, most cathode materials are compounds, and are not suited for such a chart.

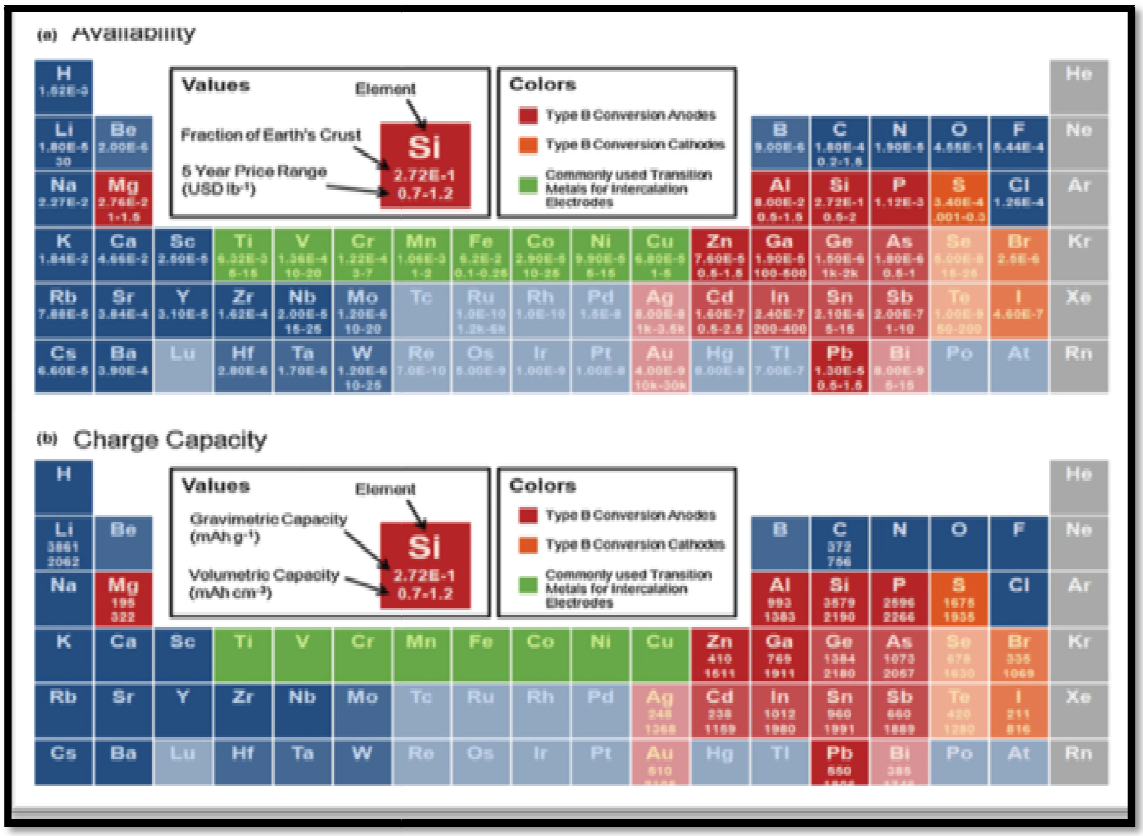



*Figure 1: (A) Availability (B) Capacities of Element That May Host Li as Electrodes. Elements with Abundance (as Fraction of Earth's Crust) below $10^{-5}$ are slightly Faded, and Elements Below $10^{-7}$ are Faded Further. Prices are Approximate 5-Year Ranges of Metal Prices (Except Ge, Which is A 3-Year Range) [32-35], 80-100 Mesh Natural Graphite for Carbon [36], and the Vancouver / USGS Prices for Sulfur [35,37], Gravemtric and Volumetric Capacities are Theoretical Values Calculated Based on Delithiated Mass and Lithiated Volume.*

However, there are still some scientific and technical problems hindering Li-S batteries to be commercialized:

- Both sulfur and lithium sulfides are intrinsically insulated, which impedes the transportation of electrons and ions.
- The volumes of cathode and anode materials change greatly during cycling process, bringing about the collapse of electrode structures.
- Lithium sulfides, as the ultimate discharge products, are in dissolvable in the electrolyte, and mostly deposit on the surface of the conductive framework.
- The intermediate discharge products lithium polysulfides ($Li_2Sn$, $4 < n < 8$) are soluble in the organic electrolyte, that will result in the loss of active materials and energy storage.

Among them, the dissolved lithium polysulfides will further diffuse to the electrolyte and form a membrane on the surface of the anode, leading to the crazing of the solid electrolyte interface film (SEI). The shuttle phenomenon gives rise to an irreversible loss of active materials, rapid capacity fading, low Coulombic efficiency, and short cycle longevity. Researchers have tried various approaches to solve this problem by virtues of delicately designed nanocarbon frameworks, such as porous carbon matrix, and so on [38-45]. They hope to take advantage of unique porous structure to prevent the dissolution, diffusion, and shuttling of polysulfides by physical encapsulation. For example, Zhang et al. designed the nested pore structure carbon with an ordered distribution of microspores and mesopores, which ensured an adequate accommodation for polysulfides to diffuse and reside evenly, and cycling performance of the device was greatly improved [38]. Park and his co-workers synthesized the honeycomb-like well-organized porous carbon nanosheets to trap lithium polysulfides [43]. Nevertheless, these physical pathways failed to immobilize polysulfides efficiently even physical encapsulation was not able to realize the practical application of Li-S batteries.

Different from the physical encapsulation, chemical adsorption displays a great potential in immobilizing poly-sulfides. Various chemical bonding approaches have been employed, in which, the functional groups and additives are introduced into carbon matrix to capture polysulfide species and prevent shuttle effect [46-51]. In this review, we show the recent advances in regard to chemical interactions between polysulfides and the functional groups or additives in Li-S batteries. Firstly, we introduce the electrochemical transportation fundamentals of Li-S cells, and then various types of functional groups and additives that utilize chemical interactions to anchor polysulfides by different sulfur hosts were discussed and analyzed. Finally, we summarize and present the challenges and prospect of Li-S batteries.

### *1.1. Fundamental of Li-S Batteries Charge/Discharge*

The conventional Li-S batteries are constituted by a cathode of sulfur, an anode of lithium metal, and an indispensable ether based electrolyte. In principle, the sulfur existing as ring-like octatomic molecules ($S_8$) will be reduced to $Li_2S$ as the final discharge product, and oxidized to sulfur reversibly when the battery was charged. The whole reaction can be represented as $S_8$+16Li8$Li_2S$. However, the actual discharge and charge processes are exceedingly complex, accompanied with many multiple side reactions simultaneously [52-57]. A schematic illustration describing the working mechanism of Li-S batteries during the cycling test and a typical galvanostatic charge/discharge profile is shown in Fig. 2. The discharge process has two or three reduction stages depending on the composition of electrolyte [55,58,59]. The first stage, a rapid dynamics reaction, takes up about a quarter of the profile, corresponding to the reduction of $S_8$ to $Li_2S_4$ at about 2.4 V [57,60]. The resulted lithium polysulfides will dissolve and diffuse into the organic electrolyte. With the discharge process going on, these high-order polysulfides will be reduced to loworder polysulfides ($Li_2Sn$, $2 < n < 4$) and $Li_2S$. The second stage accounts for another quarter of the whole discharge process with a total discharge capacity of 1316 mAh $g^{-1}$and a plateau voltage of less than 2.1 V. However, the last stage in the discharge profile matching with the further reduction of $Li_2S_2$ to $Li_2S$, is not exhibited in the cyclic voltammetry (CV) curve, which is attributed to the sloped shape and the voltage difference between the previous two stages. The dissolution and diffusion of lithium polysulfides have a serious influence on the electrochemical performance of Li-S batteries due to the following reasons [61-64]. (i) Causing the loss of active materials during cycling tests. A critical issue with respect to the polysulfides is their dissolution in organic electrolytes and the incomplete conversion of sulfur to $Li_2S$. Moreover, the dissolved lithium polysulfide species can move toward lithium anode through the separation membrane and react with lithium metal, causing the loss of active materials. (ii) Bringing in the shuttle effect. Owing to the concentration gradient, the polysulfide ions diffuse from the cathode to anode easily, and the high-order polysulfide species are reduced to low-order polysulfide species on the lithium surface. The reverse process occurs when the battery was charged. This phenomenon happening during the discharge and charge processes was named shuttle effect. The final discharge product deposited on the surface of lithium metal is $Li_2S$, which is insoluble, insulated and will increase the impedance of batteries. Therefore, the polysulfide species generated during the discharge process are harmful to Li-S cells, and it is imperative to control the solubility of the polysulfide species.

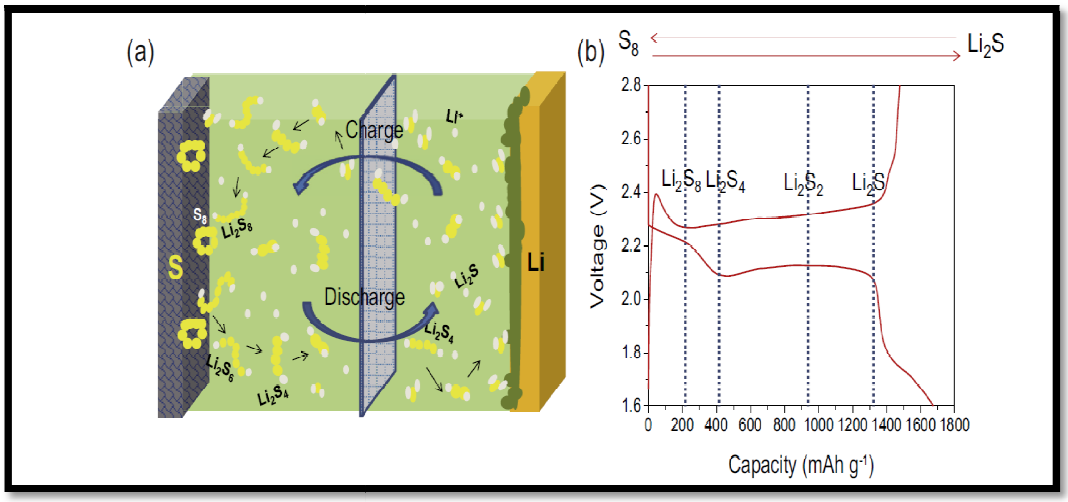



*Figure 2: (A) A Schematic Illustration of the Redox Reaction in Li-S Batteries*
*(B) Galvanostatic Charge / Discharge Profiles and thetypical chemicals in each stage.*

Figure 3 is a fairly comprehensive form of a popular chart, depicting average electrode potential against experimentally accessible (for anodes and intercalation cathodes) or theoretical (for conversion cathodes) capacity. This allows the reader to evaluate various anode and cathode combinations and their theoretical cell voltage, capacity, and energy density. The chart can also be used to identify suitable electrolytes, additives, and current collectors for the electrode materials of choice. The acronyms for the intercalation materials (Fig. 3a) are: LCO for "lithium cobalt oxide", LMO for "lithium manganese oxide", NCM for "nickel cobalt manganese oxide", NCA for "nickel cobalt aluminum oxide", LCP for "lithium cobalt phosphate", LFP for "lithium iron phosphate", LFSF for "lithium iron fluorosulfate", and LTS for "lithium titanium sulfide". To enable the application of new types of electrode materials, various strategies have been used. These strategies are summarized in Fig. 3, and are often similar regardless of type of material, crystal structure, or operating mechanism.

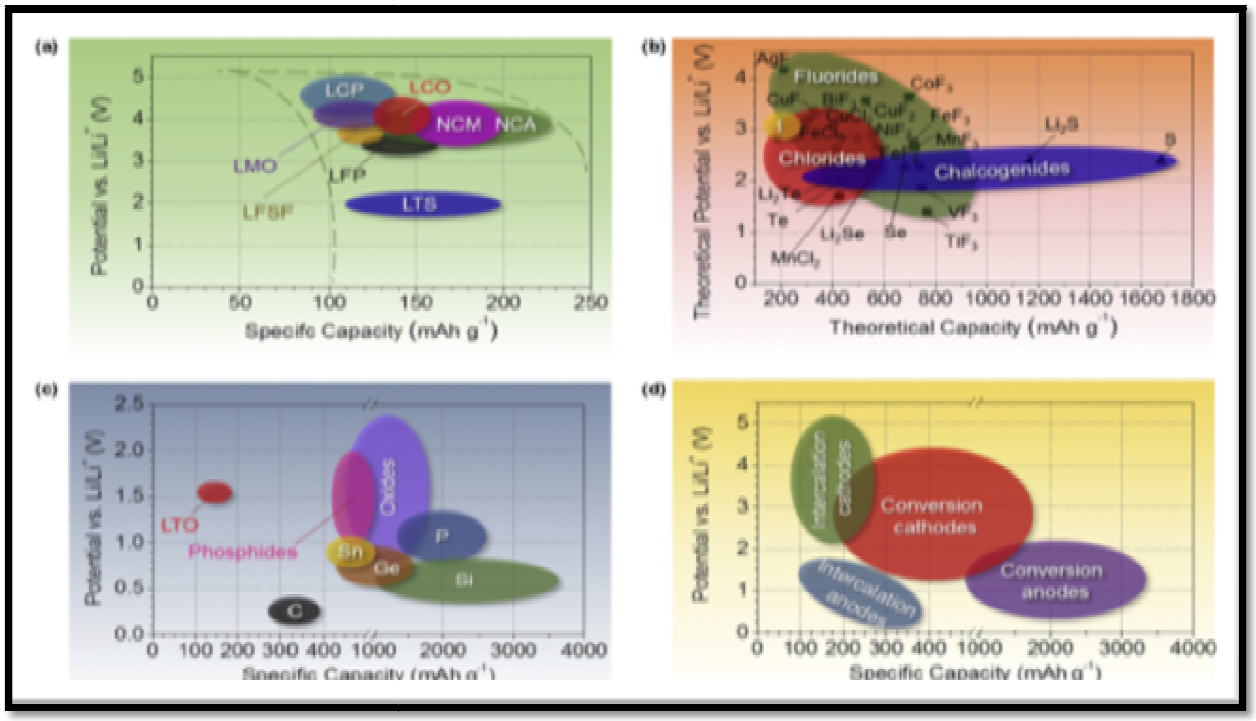



*Figure 3: Approximate Range of Average Discharge Potentials and Specific Capacity of Some of the Most Common (A) Intercalation-Type Cathodes (Experimental), (B) Conversion Type Cathodes (Theoretical), (C) Conversion Type Anodes (Experimental), and (D) an Overview of the Average Discharge Potentials and Specific Capacities for All Types of the Electrodes*

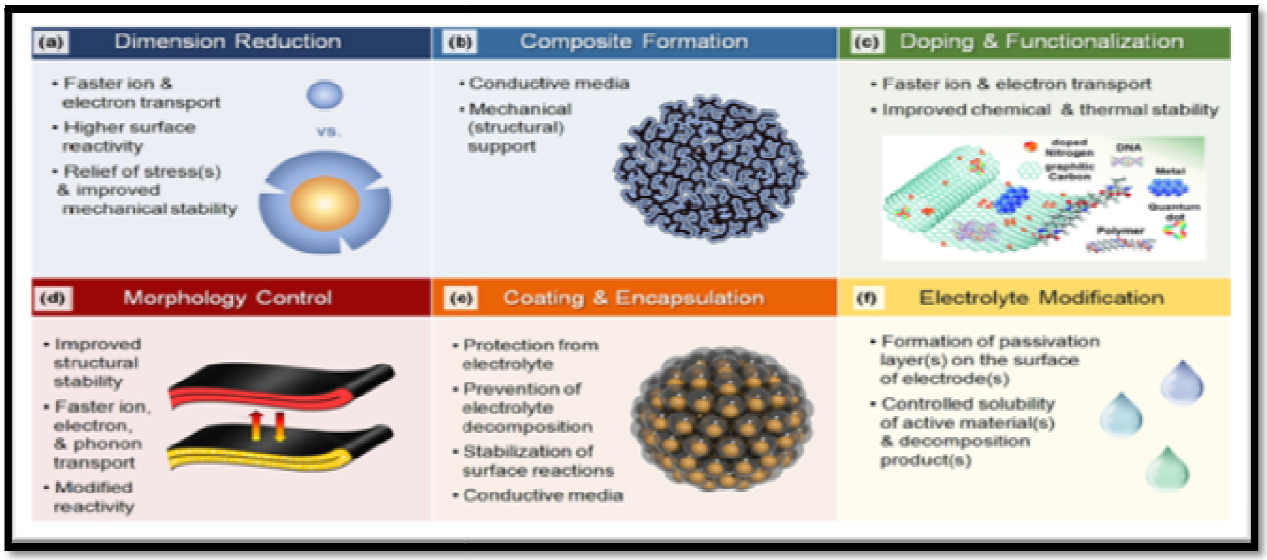



*Figure 4: General Strategies for Performance Enhancement and Their Rationale: (A) Reducing Dimensions of Active Materials, (B) Formationof Composites, (C) Doping and Functionalization, (D) Tuning Particle Morphology, (E) Formation of Coatings or Shells around Active Materials, (F) Modification of Electrolyte, Schematic Figure in (A), (B), (C) and (D) Reproduced with Figure Copyright (2014, 2016, 2017) from the Royal Society Chemistry [44], While Schematic Figure in (E), (F) Is Reproduced with Copyright (2014) from Nature Publishing Group.*

**2. The Significance of Li Metal Anode in Working Li–S Batteries**

Li metal anode plays a significant role in the service life of a Li–S battery[65].However, most of the publications are conducted in coin cells with at least 1500% lithium and 200% electrolyte excess. Few pouch cells have been declared in scientific publications. Coin-cell format is a very good stage to characterize the potential of materials applied to electrochemical cells, which constructs the best environment for material characterization. However, toward a cell for the practical applications, several applicable indicators are required, such as material cost, discharging capacity and energy density based on the whole cell, and safety performance etc. In the engineering field of Li–S batteries, it is a difficult tradeoff between the energy density (>350 Wh $kg^{-1}$) and lifespan (>100 cycles), even with the neglection of the power density. However, its role is severely neglected in a coin cell with the excess of Li metal and electrolyte. When we adopt the pouch-cellformat to evaluate Li–S batteries, the role of anode will be prominent. In the pouch-cells, the areal sulfur loading is very large to render a cell with a high energy density. However, this induces both seriousLiPS shuttle and a large current on the surface of metallic Li anode. Considering a 2000 mAh pouch cell as a typical example (an average capacity for a common smartphone), when the cell is discharged at0.2 C (1.0 C = 1675 mA $g^{-1}$, assuming the discharging capacity of 1200 mAh $g^{-1}$), the current applied to the anode is estimated at 558 mA, which is much larger than that in a coin cell (0.1 ~ 10mA). The large areal current generally cannot distribute uniformly on the anode surface [66]. Some sites of the anode surface are possible to concentrate the currents, resulting in the dendritic Li deposition and electrolyte consumption [67].The situation becomes even worse in the power battery for electric vehicles. These drawbacks seriously deteriorate the cycling performance of a Li–S battery.

Generally, the disastrous effects of dendritic Li growth operated at high currents include Li metal powdering and electrolyte exhaustion, finally causing the cell failure (Figure 4) [68].

- At the large current, dendrites are easy to nucleate and continuously grow. Due to the side reactions between Li metal and electrolyte/LiPSs, the dendritic Li becomes dead and powdery Li with the SEI (solid-state electrolyte) wrapping outside after several repeated plating/stripping processes[69]. The powdery Li possesses a large surface area and thus a large tendency to catch fire if meet the air, which induces safety concerns [70]. The dead Li is covered by a thick SEI(solid-state electrolyte) layer and its reactivity will be substantially reduced after many cycles[71]. Therefore, the less cycled Li–S batteries are more dangerous than the failed one.
- The dendritic and powdery Li presents a strong reactivity with the electrolyte. Electrolyte exhaustionis widely observed in a long-cycled Li–S pouch cell. The loss of interconnected ionic channels directly leads to the cell failure [72]. However, it is not the decisive reason for the cell failure. When freshelectrolyte is injected into the failed cell, the cell regains discharge capacity (Figure 5a) [69]. However, the fresh electrolyte still cannot preservethe high capacity and this 'twice born' cell gets rapid capacitydecay. Another 'twice-born' cell with cycled cathode vs. fresh anode is fabricated. The cell indicates an improved discharging capacity from 314 to 1030 mAh $g^{-1}$ (Figure5b) at 0.1 C and remains stablein the following cycles (999 mAh $g^{-1}$ at 15$^{th}$ cycle) [69]. Therefore, Li metal anode itself is the fundamental factor to decide the cell failure.

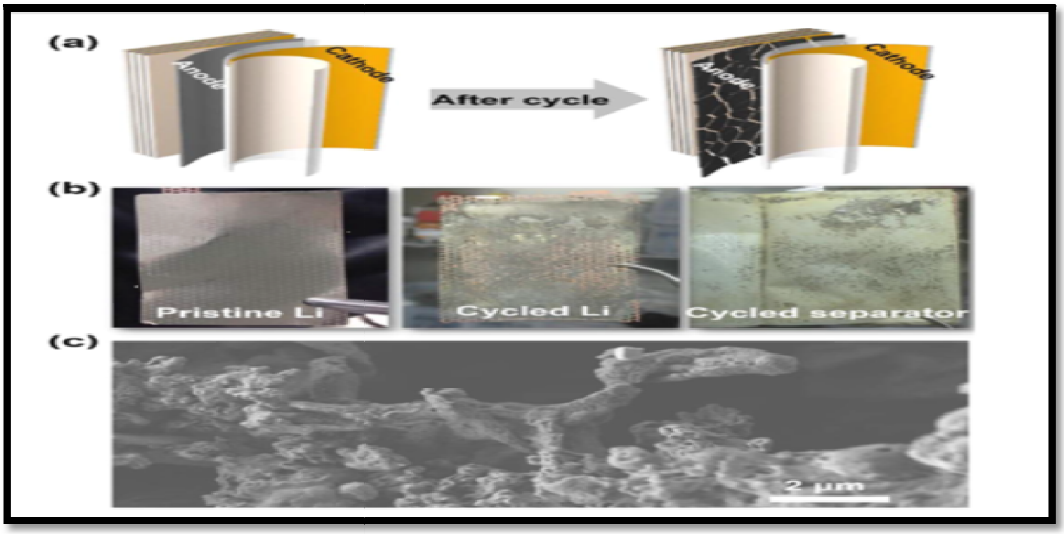



*Figure 5: Morphology of Li Metal Anode in A Li–S Pouch Cell, (A) the Schematic Diagram for Li Metal Anode Evolution during Repeated Cycles, (B) Digital Images of Pristine Li Metal Electrode, Cycled Li Metal Electrode and Cycled Separator(C) SEM Image of a Cycled Li Metal Anode, (A–C) Reproduced with Permission from Ref. [69].*

Further analyzing the cycling performance of the Li–S battery, an obvious relation is observed between the discharging capacity and voltage evolution. The time point for rapid capacity decay is the samewith that of voltage fall-off (Figures 6c and 6d). Consequently, the large polarization induced by powdery and dead Li is the primary reason for the cell failure. A similar conclusion has been reachedby Xiao and colleagues through comparing the Li anodes cycling at different rates after 100 cycles (Figure 6)[73].When the current density increases from 0.2 to 0.5, 1and 2 C, the thickness of porous Li layer expands from 100 to 160, 223, and 270 μm, respectively, hence leading to the polarization aggravation and capacity decay. A novel failure mechanism of Li metal anodes is found that porous layer of the dead Li grows inward to the bulk (fresh) Li metal anode, evolving to a highly resistive layer with mossy Li. This porous dead Li layerleads to huge transfer resistance and cell polarization [74]. Before the dendrite-induced short circuit, the impedance of the battery sharply escalates and hence the service life is early terminated.Therefore, Li metal anode is critical to the degradation of a practical Li–S battery, especially in the pouch-cell format. Dendritic Li growth induced by the large currents is mainly responsible for the cell failure [75]. Other than the usually prevailing theory of the failure caused by dendrite-induced short-circuit, the practical cell is more possible to be failed by the large polarization caused by powdery and dead Li in the porous layer. In a Li metal battery with the highly stable cathode (such as lithium iron phosphate and lithium titanate), the large capacity decay of Li metal battery is primarily due to the considerable polarization resulting from the porous and highly resistant layer inthe Li metal anode. This conclusion is especially valid in a Li–S battery, where the LiPSs can readily react with Li dendrites to obtain the powdery, mossy, and dead porous Li layer[76]. Consequently, it is rather indispensable to construct a stable and compact SEI film to protect the Li metal anode in a Li–S battery from the corrosion of LiPSs andelectrolyte.

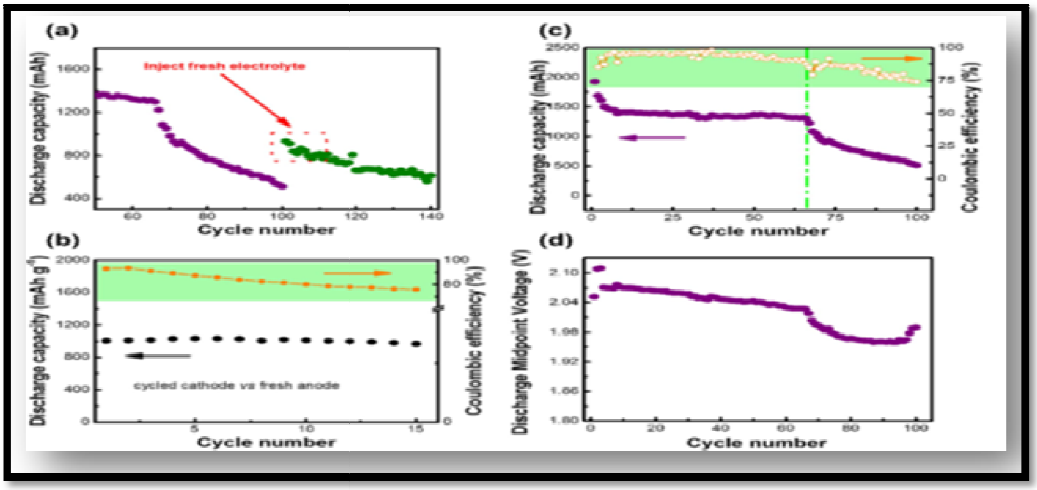



*Figure 6: Failure Mechanism of A Li–S Pouch- Cell. Cycling Performance of the Twice-Born Cells (A) After Injecting Fresh Electrolyte and (B) after Changing to Fresh Li Metal Anode. (C) Cycling (B) Performance of a Li–S Pouch Cell and (D) Its Corresponding Voltage Evolution. (A–D) Reproduced With Permission From Ref. [68].*

Anode materials are necessary in Li-ion batteries because Li metal forms dendrites which can cause short circuiting, start a thermal run-away reaction on the cathode, and cause the battery to catch fire. Furthermore, Li metal also suffers from poor cycle life. While the major efforts to enable Li metal anodes have been reviewed by others [77], this topic will not be covered herein. Instead, this section provides a concise overview of secondary anode materials. For further investigation, we recommend other more detailed reviews on carbon [78], lithium titanium oxide (LTO) [79,80], and Type A and Type B conversion anode materials [81–83].

*2.1. Graphiticand Hard Carbons*

The carbon anode enabled the Li-ion battery to become commercially viable more than 20 years ago, and still is the anode material of choice. Electrochemical activity in carbon comes from the intercalation of Li between the graphene planes, which offer good 2D mechanical stability, electrical conductivity, and Li transport (Figure8a). Up to 1 Li atom per 6 C can be stored in this way. Carbon has the combined properties of low cost, abundant availability, low delithiation potential vs Li, high Li diffusivity, high electrical conductivity, and relatively low volume change during lithiation/ delithiation (Table 1). Thus carbon has an attractive balance of relatively low cost, abundance, moderate energy density, power density, and cycle life, compared to any other intercalation-type anode materials. Carbon's gravimetric capacity is higher than most cathode materials (Figure3), but the volumetric capacity of commercial graphite electrodes is still small (330–430 mAh $cm^{-3}$).

Commercial carbon anodes can be largely divided into two types. Graphitic carbons have large graphite grains and can achieve close to theoretical charge capacity. However, graphitic carbons do not combine well with a propylene carbonate (PC)- based electrolyte, which is preferred due to a low melting point and fast Li transport. PC intercalates together with the $Li^+$ between the graphitic planes, causing the graphite to exfoliate and lose capacity [84]. Even without solvent intercalation, Li intercalation occurs at the basal planes, and thus the SEI also preferentially forms on these planes as well [85]. During Li intercalation, single crystalline graphitic particles undergo uniaxial 10% strain along the edge planes [86,87]. Such large strain may damage the SEI and reduce the cell's cycle life. Recently, graphitic carbons have been coated with a thin layer of amorphous carbon [88,89] to protect the vulnerable edge planes from electrolyte and achieve high coulombic efficiency. Hard carbons have small graphitic grains with disordered orientation, and are much less susceptible to exfoliation. These grains also have an voids between them, resulting in reduced and isotropic volume expansion. Nanovoids and defects also provide excess gravimetric capacity, allowing capacity in excess of the theoretical 372 mAh $g^{-1}$[78,90–92].

Together, these properties make hard carbons a high capacity high cycle life material. However, the high fraction of exposed edge planes increases absolute quantity of SEI formed, reducing the coulombic efficiency in the first few cycles. Given that a full Li-ion cell has a limited Li inventory, this represents a serious disadvantage in terms of achievable capacity. Also, the void spaces significantly reduce the density of the particles, further decreasing volumetric capacity. Finally, impurities such as hydrogen atoms can also provide extra capacity in carbon based anodes [93]. However, such electrodes suffer from larger voltage hysteresis, higher irreversible capacity loss, and even lower volumetric capacity, and thus are unlikely to be commercialized [92].

| Material | Lithiation Potential (V) | Delithiation Potential (V) | D ($Cm^2 S^{-1}$) | Volume Change |
|---|---|---|---|---|
| Graphite | 0.07,0.10,0.19 | 0.1,0.14,0.23 | $10^{-11}$-$10^{-7}$ | 10% |
| LTO | 1.55 | 1.58 | $10^{-12}$-$10^{-11}$ | 0.20% |
| Si | 0.05,0.021 | 0.31,0.47 | $10^{-13}$-$10^{-11}$ | 270% |
| Ge | 0.2,0.3,0.5 | 0.5,0.62 | $10^{-12}$-$10^{-10}$ | 240% |
| Sn | 0.4,0.57,0.69 | 0.58,0.7,0.78 | $10^{-16}$-$10^{-13}$ | 255% |
| $Li_2O$ | N/A | N/A | $5\times10^{-12}$-$5\times10^{-10}$ | N/A |

*Table 1: Properties of Some Commonly Studied Anode Materials [78-97].*

*2.2. Lithium Titanium Oxide ($Li_4Ti_5O$/LTO)*

LTO has been successfully commercialized because it allows the combination of superior thermal stability [94], high rate, relatively high volumetric capacity, and high cycle life, despite the higher cost of Ti, the reduced cell voltage, and lower capacity (175 mAh $g^{-1}$& 600 mAh $cm^{-3}$ theoretical). High rate and stability originates from a ''zero strain'' intercalation mechanism in combination with a high potential of lithiation. LTO is considered ''zero strain'' because the phase change caused by lithiation/ delithiation only results in a slight (0.2%) change in volume [95–97]. Electrochemically, this manifests itself as a small voltage hysteresis in its charge–discharge profile (Figure8d). In addition, a high equilibrium potential (-1.55 V vs. $Li/Li^+$) allows LTO to be operated in a potential window above 1 V, largely avoiding the formation and growth of the anode SEI, which can slow Li insertion and induce Li losses in graphite anodes (Table 1). Even when an SEI is formed, the lack of volume change enhances the SEI's stability. Since SEI impedance is not an issue, LTO nanoparticles can be used, similar to intercalation cathode material, which lead to higher rate performance at the expense of lower volumetric capacity [98,99]. In addition, LTO is extremely safe because its high potential prevents Li dendrite formation, even at high rates. Thus, although LTO does not have particularly high Li diffusivity or electrical conductivity, it is a good material for lower energy, but high power high cycle life Li-ion metal batteries. Unfortunately, surface reactions are not completely avoidable with LTO anodes. LTO suffers from severe gassing due to a reaction between the organic electrolyte and the LTO active material [100]. This reaction can be suppressed by carbon coating, but

carbon can also catalyze and accelerate electrolyte decomposition in the formation of an SEI, especially at high temperatures [101,102]. Even so, LTO anodes can last for tens of thousands of cycles giving this electrode a distinct advantage over most other anode materials for high power applications [103,104].

*2.3. Conversion Materials – Alloying Materials (Type B)*

Here, 'alloying materials' refer to elements which electrochemically alloy and form compound phases with Li (i.e. Type B conversion materials as in Eq. (2)) at a low potential (preferably below 1 V). Alloying materials can have extremely high volumetric and gravimetric capacity, but are notorious for their colossal volume change, expanding to several times the original volume upon lithiation (Figure8c illustrates how this occurs for Si). This can cause particles to fracture and lose electrical contact [105]. For anodes, volume change can destroy the SEI protective layer, resulting in continuous electrolyte decomposition, loss of Li inventory and increasing cell impedance. Alloying anodes thus generally suffer from short cycle life due to the loss of active material [106] and increasing cell impedance [107], especially at high mass loadings. In general, the most successful strategy has been to produce a carbon composite in which the particles of alloying material have sufficiently small dimensions for mechanical stability, electron transport, and Li transport, while maintaining Li diffusion paths within the electrode (which commonly requires a hierarchical structure such as Figure 3b[108]). To stabilize the SEI, the active material can be encapsulated in a carbon shell with a sufficient void space to allow for volume expansion (Figure 3e) [109–114]. This may, in principle, stabilize the SEI and prevent particles from sintering into larger particles, enabling high cycle life even at high mass loadings [115]. Electrolyte additives can further stabilize the SEI and prolong the cycle life [116 –118], and binders which bond to the active material, have high stiffness and swell minimally in electrolytes can provide additional mechanical stability if a carbon shell is not used [119–123]. Even so, high mass loading electrodes with high (>800 mAh $cm^{-3}$) volumetric capacity and long cycle life ($10^3$ +cycles) in full Li-ion metal battery cells have yet to be demonstrated. Also, nanoparticles inherently have high surface area, which result in large quantities of SEI formation and large irreversible capacity loss during the initial cycles. Of all alloying materials, Si has received the most attention due to its relatively low average delithiation potential, extremely high gravimetric and volumetric capacity, abundance, lost cost, chemical stability, and non-toxicity. Sn has also been of high interest, having similar properties except with lower gravimetric capacity, slightly lower cell voltage, but higher electrical conductivity. However, Sn appears to suffer from easy fracturing (Fig. 3a), even when the particle dimensions are decreased to the 10 nm range [124]. Ge does not fracture even at larger particles sizes [125,126], but is too expensive for most practical application (Figure 1a). Ga also has an interesting property of being liquid near room temperature [127], but is again too expensive. Of the cost effective Li alloying metals, Zn, Cd, and Pb have good volumetric capacity, but suffer from low gravimetric capacity. Al also suffers from severe fracturing even with nano dimensions, as confirmed by in situ transmission electron microscopy (TEM) [128]. P and Sb have received some attention in recent years. Both elements have good capacity, and well performing electrodes have been constructed by merely ball milling the material with carbon [129,130]. However, both elements are toxic, have relatively high delithiation potentials, and Sb is additionally not very abundant (Figure 1). Phosphorus is also particularly dangerous due to its potential to form phosphine.

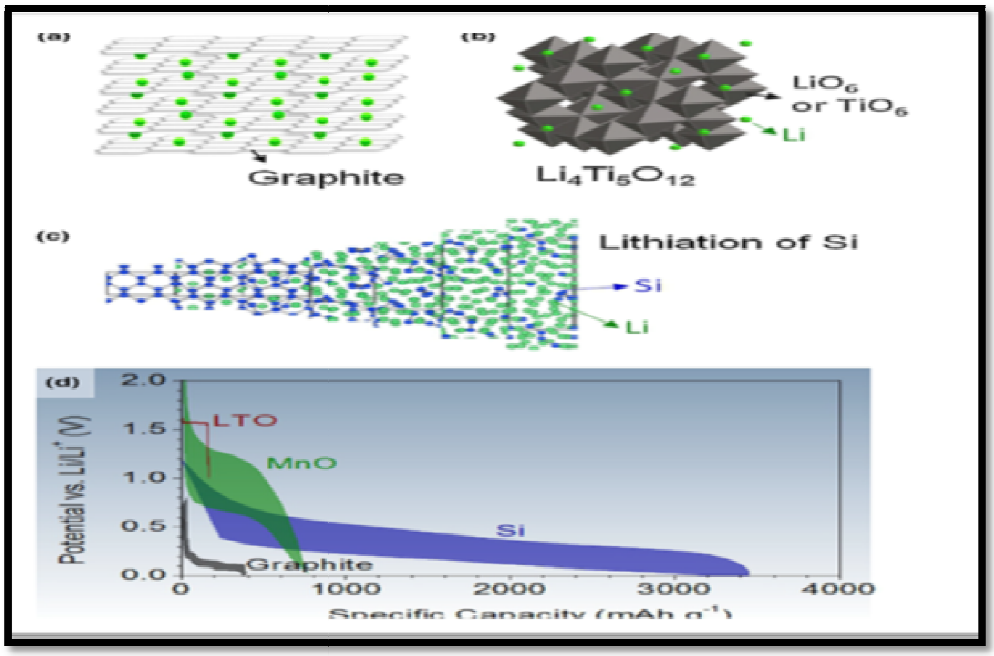



*Figure 7: Crystal Structure of (A) Lithiated Graphite [131], (B) Lithium Titanate (LTO) [132], and (C) Silicon During Lithiation [133](Reproduced with Permission Copyright (2014) American Chemical (D) Society) and (D) Charge- Discharge Profiles at Low Charge/Discharge Rates, Showing (E) Voltage Hysteresis [134-136]*

*2.4. Conversion Materials – Other (Type A)*

In the past, one popular approach to developing conversion materials was to use oxides in which $Li_2O$ are formed on the initial charging of the battery. The $Li_2O$ acts as a 'glue' to keep particles of the alloying material (such as Si or Sn) together [137], while also reducing the overall volume change within particles. However, $Li_2O$ has low electrical conductivity, and this approach inevitably results in a large irreversible capacity and a large voltage hysteresis, much of which remains even at extremely slow rates [138]. Alternatively, the $Li_2O$ itself can be used as an active material if the voltage range is significantly widened, enabling the use of non-alloying transition metals (such as Manganese (II)Oxide, Figure 8d). This reduces the first cycle capacity loss and increases the charge capacity, but has the obvious issue of further reducing the potential difference with the cathode. Also, if the $Li_2O$ phase is consumed, the nanoparticles of active alloying materials can sinter into larger particles and increase resistance [139,140]. Furthermore, the process generally also results in large volume change, causing issues similar to alloying anodes. Of the various Type A conversion anode materials, $MgH_2$ and $Li_{1.07}V_{0.93}O_2$ are interesting in that they both have relatively small voltage hysteresis and delithiation potentials, although at low rates [141,142]. However, no studies have shown that these electrodes are viable at higher rates, and the demonstrated cycle life is short as well. Similarly, some phosphide and nitride electrodes have been shown to have relatively low voltage hysteresis, but only at low charge/discharge rates for several cycles [143].

**3. Advanced Cathode Materials**

Advanced Cathode Materials also play an important role in LIBs. Lithium oxides compounds were well developed by scientist in 1980. Crystallization of lithium oxides compounds could provide fair lithium ions mobility during the redox reaction. Cathode materials especially oxides compounds have a stable crystal structure and minimum volume expansion during lithiation and delithiation process. They have good adaptability at an entire voltage range of lithium insertion and extraction,so it can provide a good cyclic performance. Nowadays, more and more novel cathode materials based on high energy density attracted attention from researchers, such as lithium-sulfur batteries system and lithium air batteries system.

*3.1. Lithium Cobalt Oxide ($Licoo_2$)*

$Li_xCoO_2$ becomes the well-known cathode electrode materials with good conductivity and Li ion mobility in LISBs for decades. Todays, it is still a widely commercial used cathode material for LISBs. In theoretical, lithium cobalt oxide has a high specific capacity with 274 mAh/g with respect to full delithiation of Li ion extraction and producing $CoO_2$[144],but in reality, full lithiation is not reversible process in $Li_xCoO_2$. In practical, x=0.5 induced capacity loss with value of 140mAh/g [145]. Also layered compounds structural is a significant characteristic for $LiCoO_2$. It is most widely accept cathode materials in LISBs.

*3.2. Lithium Iron Phosphate (LFP)*

(LFP) is another commercialized cathode materials with olivine structure in lithium ion sulfur batteries. It still attracted attention from researchers due to the inexpensive and naturally abundant,but low ionic and electrical conductivity are major disadvantages for LFP,so to improve high rate capability and long cyclic performance by carbon coating, size reduction and morphology modification still are research interests for researchers[146].Besides, mechanism of phase transformation during lithiation and delithiation process is another research interests of Lithium-Air Batteries[147]. One of the novel cathode materials research recent years in LIBs is lithium-air batteries. The cathode lithium oxygen reaction can provide a high theoretical capacity of 3.5 Kwh/kg nonaqueous lithium oxygen battery[148]. The major cathode product material is lithium peroxide. The cathode oxygen reduction reaction (ORR) is $O_2 + 2Li^+ + 2e^- \rightarrow 2Li_2O_2$, which has overall equilibrium potential of 2.96V versus lithium metal. However, the poor cyclic performance, slowly charging/discharging rate, high overpotential and low energy efficiency are major problems for lithium-air batteries. Generally, the lithium air batteries performance highly depends on the products created in cathode during lithiation and delithiation process. The morphology of cathode reaction products, the morphology of peroxide effect on batteries performance and fabricated high performance cathode are hot research topics on lithium air batteries[149]. According to literature and Figure.7, there are many approaches to design an ideal cathode for lithium air batteries[150]. For instance, the porous structures with appropriate pore size, to improve reaction kinetics by catalyst and oxygen diffusion and to improve electrical conductivity are major strategies.

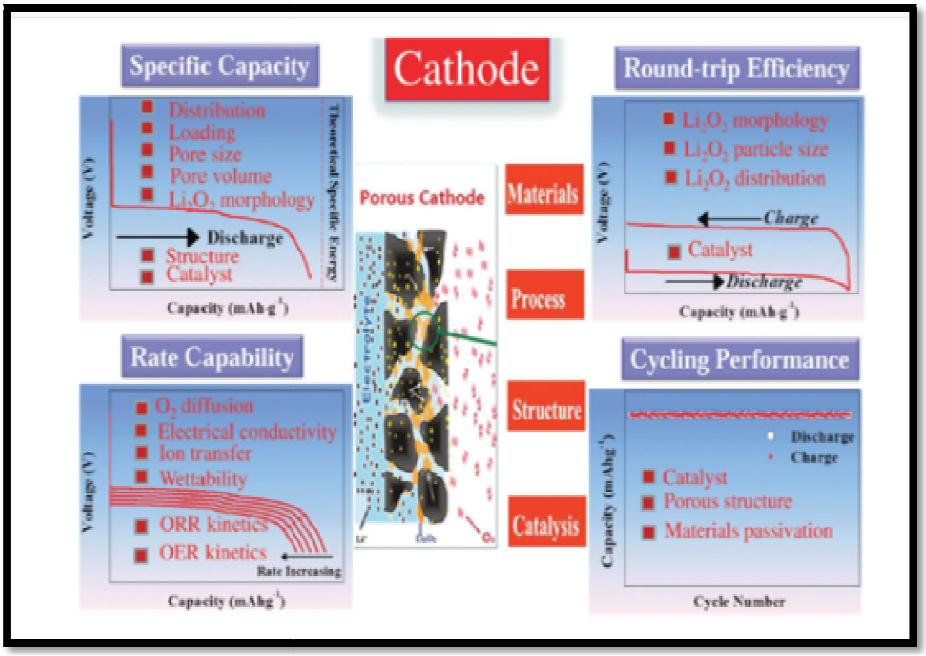



*Figure 8: Ideal Cathode Designing for Lithium-Air Batteries [150].*

*3.3. Challenges of a Sulfur Cathode*

The significant advantages of sulfur as a positive electrode are evident, but wide-scale commercial use is so far limited because of some key challenges that must be addressed. The first main issue is that sulfur is both ionically and electrically insulating [151]. The insoluble low order lithium polysulfide discharge products are also expected to be electronic insulators, although their properties are uncertain as they have not been isolated as single phases. To overcome the insulating nature of these materials, intimate contact of conductive additives such as carbon or metals with high surface areas (i.e. nano-sizing) [152] augment the electrical conductivity, and organic electrolytes that wet the sulfur create pathways for ionic transport. Through reducing the sulfur particle size, the diffusion path for electrons and lithium ions is greatly reduced and leads to a higher utilization of the active sulfur mass. These are not the only challenges in the Li-S cell. Most of the problems arise because of the intermediate discharge products ($Li_2S_x$, $2 < x < 8$). Upon reduction by lithium in an organic electrolyte, sulfur is reduced stepwise to a sequence of highly soluble lithium polysulfide intermediates. These intermediates can diffuse through the electrolyte to the lithium metal negative electrode where they are reduced further to insoluble $Li_2S_2/Li_2S$ which can form dendrites and reduce the active lithium surface area[152,153] Once this insulating layer is formed on lithium, subsequent higher order polysulfides ($S_n$) present in the electrolyte can become reduced at this surface to lower order polysulfides ($S_{n-x}$). $S_{n-x}$ ions can diffuse back to the positive electrode where they are reoxidized to $S_n$. The diffusion of lithium polysulfides between the electrodes is termed the "sulfur shuttle mechanism" and is a major cause of active mass loss, low Coulombic efficiency (excess energy required to charge the cell than obtained from discharge of the cell) and self-discharge (discharge of the cell when no load is applied) in a Li-S cell. The last main issue with the Li-S cell are the low order insoluble final discharge products $Li_2S_2/Li_2S$. These can form on the exterior of the electrically conducting host that is mixed with sulfur and build-up over many cycles to form highly insulating agglomerates that increase impedance and cause active mass loss[154,155].

*3.4. Contained Cathodes*

3.4.1. Macro/Meso/Microporous Carbon

In order to effectively house sulfur, the host must contain the sulfur without significantly diminishing the overall practical properties of the cell, i.e. the gravimetric/volumetric energy density. The optimal material to satisfy these conditions is lightweight, conductive and can "wire-up" the insulating sulfur, such as one made predominately of carbon. This configuration was used in the earliest reports, but it failed to harness the potential of carbons to limit polysulfide dissolution by trapping sulfur and its reduced species at the positive electrode owing to primitive carbon architecture. Carbon is highly effective as an electronic conduit to enable redox accessibility of the sulfur but it can also act as a framework to encapsulate the redox products. A straightforward solution is to introduce pores in the carbon that sulfur can impregnate. Pore size is defined by the IUPAC as being macro (> 50 nm), meso (2 – 50 nm) or micro (< 2nm). Various carbons embodying these pore structures and their combinations have been employed recently with varying degrees of effectiveness. Macroporous carbons have been the least utilized for Li-S cells owing to their open architecture which is highly ineffectual at containing soluble polysulfides. However, if the macroporous carbon is coupled to a high viscosity electrolyte, the lithium polysulfides are limited in mobility and will predominately remain at the positive electrode. Watanabe et al. used an ordered inverse opal carbon to house sulfur and replaced the commonly used low viscosity organic electrolytes with a high viscosity glyme-Li salt[156].This electrolyte is similar to a room temperature ionic liquid

capacity of 6 over 700 mA h $g^{-1}$ sulfur after 50 cycles and a Coulombic efficiency of 97%. While the results are promising, the current density was low (139 mA $g^{-1}$ sulfur) and the poor scalability of inverse opal carbons is problematic for large-scale applications. Most of the recent reported research on porous carbon positive electrodes has focused on mesoporous carbons (MC's), following on early work by the Nazar group where small carbon mesopores (3-4 nm) and a hydrophilic polymer coating provided effective confinement of sulfur and its reduction products to yield high reversible capacities up to 1320 mA h $g^{-1}$ sulfur[157].A question concerns what pore size and distribution are optimal. Liu et al. have used a systematic approach to determine the effect that both pore size and sulfur loading89 have on the cycling stability and overall capacity of the Li-S cell[158]. A series of MC's with tunable pore sizes (3, 7, 12 and 22 nm) and pore volumes up to ~4.8 cm 3 $g^{-1}$ were synthesized using a hard template approach. The sulfur was infiltrated into the various MC's at different weight ratios using a two-step infiltration technique. Sulfur dissolved in carbon disulfide was mixed with the MC and once dry, the composite was heated at 155 °C where the low sulfur viscosity permits flow into the carbon pores. The weight fraction of sulfur gradually increased as the pore size of the MC increased, and a sulfur content of 83 wt% was reported for the 22 nm MC material. Surprisingly, all of the sulfur/carbon composites exhibited almost identical initial sulfur utilization even though the weight ratio of sulfur was significantly different (56 wt% to 84 wt%) between MC's. Contrary to other reports, this suggests there is no influence on the battery performance even if the MC is fully "stuffed" with sulfur. The MC with the largest pore size/volume clearly should be used to optimize both gravimetric and volumetric capacities were this to be the case. Another method of sulfur entrapment is to utilize a bimodal MC as the sulfur host. The first demonstration of this concept by Dudney et al. used a hierarchically structured sulfur-carbon nanocomposite material as the high surface-area positive electrode[159]. A porous carbon with a uniform distribution of mesopores of 7.3 nm was synthesized through a soft-template synthesis method, followed by KOH activation to result in a bimodal porous carbon with added micro porosity of less than 2 nm to the existing mesopores while maintaining integrity of the original carbon. More recent work has created bimodal carbons using a double template approach to directly fabricate highly ordered carbons with pore size split between ~6 nm and ~2 nm pores[160,161]. Each pore contributes an equal amount of pore volume with the smaller pores existing in the walls of the larger ones. When sulfur was impregnated into the carbon host, the smaller pores preferentially filled first (Figure 8a). This optimized the use of the smaller supermicropores to entrap the sulfur while the larger pores facilitated electrolyte ingress throughout the structure. An improvement on this concept was demonstrated by creating spherical bimodal-carbon particles around 300 nm in dimension with the same pore distribution (Figure 8b). Nazar et al. were able to cycle these sulfur/carbon electrodes at a high current rate of 1C and maintain a high and relatively stable discharge capacity of 850 mAh $g^{-1}$ sulfur at the 100$^{th}$ cycle (Figure 8c)[162].

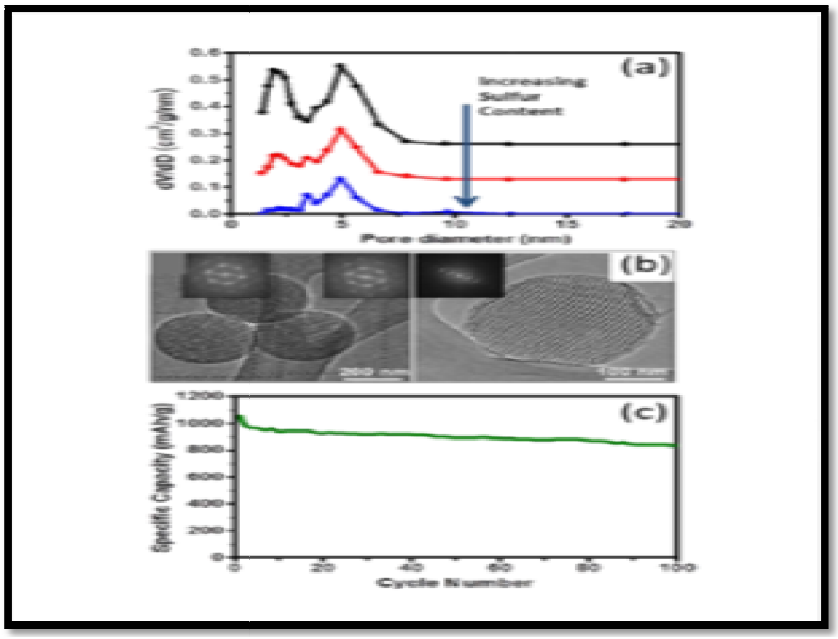



*Figure 9: A) Pore Size Distribution ofthe Bimodal Mesoporous Carbon (BMC) with Different Sulfur Loadings [160] B) TEM Micrographs of Spherical BMC Nanoparticles Showing the 2-D Hexagonal Structure [162], C) Cycling Performance ofBMC Nanoparticles with 70 Wt % Sulfur at1C Rate [162].*

Another approach similar to creating a bimodal pore structure has been achieved by Archer et al. with the synthesis of hollow carbon spheres that exhibit a porous outer shell with small 3 nm pores and a large interior cavity around ~200 nm[163].While this may not be considered bimodal in most respects, it effectively creates an enclosed area wherethe sulfur can be stored and polysulfides have difficulty diffusing out because of the small pores in the carbon shell. The hollow carbon spheres were reported to hold 70 wt% sulfur and they retained 91% of their initial capacity (1071 mA h $g^{-1}$ sulfur) after 100 cycles at a moderate C/5 rate. Possible drawbacks to the hollow carbon spheres are the fragility of the porous carbon shell and scalability of the process. A vapour infusion method is required for sulfur impregnation

involving three separate passes to obtain a high sulfur loading. Microporous carbons have also been used as hosts for sulfur in Li-S cells. Gao et al. used sucrose as a carbon precursor to form microporous carbon spheres with a very narrow pore size distribution of less than 1 nm[164]. Their material exhibited highly stable cycling with 42 wt% sulfur loading and high capacity above 900 mAh $g^{-1}$ sulfur. However, an increase in sulfur content to just 51 wt% dramatically decreases the discharge capacity by ~600 mAh $g^{-1}$ sulfur. The material also exhibited an unusual discharge profile that did not have the characteristic two voltage plateau evident in most other Li-S reports. This may be due to reaction of the carbon with sulfur to form a bonded carbon-sulfur composite owing to heat treatment, or the alkyl carbonate electrolyte mixture chosen for this work. Recent studies performed by Abruña et al. show that carbonate based solvents undergo side reactions in the presence of nucleophilic sulfide anions [165]. Activated carbon (AC) (in the form of fibres woven into a cloth) has also been examined by Aurbach et al., as a microporous host for sulfur that, uniquely, does not require binder[166]. An inexpensive commercial AC cloth with high surface area (2000 $m^2$ $g^{-1}$) and narrow pore size distribution (< 2 nm) was impregnated with 33 wt% sulfur and cycled at an intermediate current density of 150 mA $g^{-1}$ sulfur. A large, stable discharge capacity of 1057 mA h $g^{-1}$ sulfur was obtained with a very high Coulombic efficiency. The latter is aided by the use of $LiNO_3$ in the electrolyte to passivate the negative electrode and limit the sulfur shuttle mechanism.

3.4.2. Graphene

It was only a matter of time before arguably the most popular material of the past decade was coupled to sulfur in a Li-S battery. Graphene's advantageous properties of very high conductivity, large surface area and the ability to tune the hydrophobicity/hydrophilicity with surface functionalization has led to a few different methods of marrying it with sulfur to make effective electrodes [167-172]. Two different designs for sulfur/graphene composites have been employed with each having its positive characteristics. The first method utilizes large sulfur particles enveloped by graphene/graphene oxide sheets with either a polymer layer buffering the sulfur [168], or with the sulfur particles simply in intimate contact with the graphene[170,171]. The sulfur particles grown with a polymer coating followed by a graphene layer showed an ability to be cycled over 140 cycles at a C/2 rate while maintaining a discharge capacity above 500 mAh $g^{-1}$ sulfur (Figure 9a) [168]. A similar procedure was used to form a graphene oxide/sulfur composite with a final heat treatment step to melt sulfur into the 3D disordered graphene oxide (GO) sheets [170]. This composite exhibited extremely stable cycling using an ionic liquid/poly (ethylene glycol) dimethyl ether (PEGDME) electrolyte at C/10 rate with a reversible capacity of 950 mAh $g^{-1}$ sulfur over 50 cycles (Figure 9b).

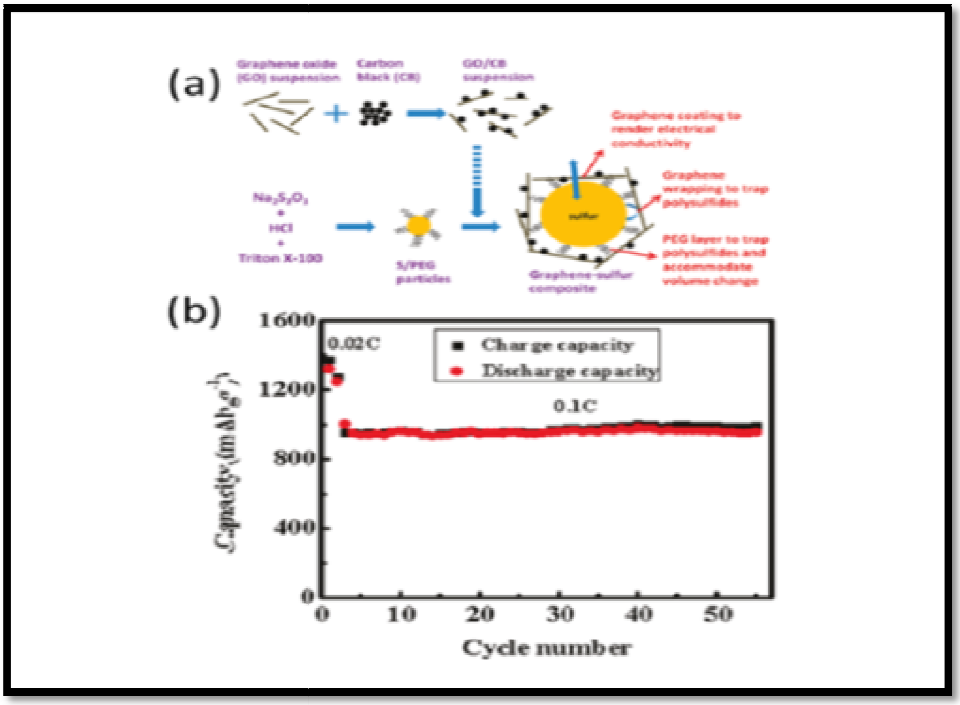



*Figure 10: A) Schematic Illustration of the Synthesis Process to form Grapheme/Polymer Coated Sulfur Particles [168]. B) Cycling Performance of A Grapheme Oxide / Sulfur Composite Using an Ionic Liquid/PEGDMEElectrolyte at 0.1C Rate [170].*

Another approach to combine sulfur and graphene is to sandwich sulfur particles between functionalized graphene sheets and apply a Nafion™ coating. This is proposed to significantly limit sulfur loss from the positive electrode owing to repulsive interactions of the Nafion $SO_3$ - moieties with the polysulfide anions that restrict diffusion into the electrolyte[169]. Thermally expanded graphite oxide is also effective as a 3D network; we note that 60 wt% sulfur that is melt-infiltrated exhibits a high initial discharge capacity of 1210 mAh $g^{-1}$ sulfur and maintains 73% capacity retention over 70 cycles at a current density of 280 mA $g^{-1}$ sulfur[172]. Graphene and graphene oxide are very promising hosts for sulfur

architectures that can be constructed around sulfur particles or melt-diffused sulfur to form sandwiched/interleaved composites.

3.4.3. Carbon Nanotubes/Fibers

Multi-walled carbon nanotubes (MWCNT) in a Li-S cell have long been investigated as a highly conductive form of carbon that might provide an encapsulation effect for sulfur due to their 1D porous structure. Jin et al. used a precipitation technique to infiltrate sulfur into the large pore of MWCNT's by oxidation of sodium polysulfide species in the presence of MWCNT's [173].The composite exhibited high initial sulfur utilization but had fairly rapid capacity fading over thirty cycles with only 63% capacity retention. This suggests that MWCNT's have a very limited effect at retaining soluble polysulfides. Limitations occur because of their 1D structure and a typical length on the order of a few microns which limits Li-ion diffusion compared to a more open 3D network. However, recent work that features a new method of infiltrating sulfur into disordered carbon nanotubes (DCNT's) holds promise. Wang et al. formed DCNT's from polyaniline deposited in an anodized alumina membrane (AAO)[174]. The sulfur was incorporated into the DCNT's through a vapour infusion method whereby smaller sulfur molecules ($S_2$) could theoretically penetrate further into the carbon structure and possibly even penetrate graphitic layers. Various impregnation temperatures under vacuum were attempted, with 500 °C proving optimum for stable cycling and providing composites with 40 wt% sulfur active mass. Several hurdles remain as there is a significant irreversible capacity in the first few cycles which is due to excess sulfur on the surface of the DCNT's.

Carbon nanofibers (CNF's) have also been investigated as conductive additives[175] to carbon/sulfur composites, or more importantly utilized in a similar fashion to the DCNT's discussed previously. Zhang et al. used porous CNF's synthesized by electrospinning a polyacrylonitrile/polymethyl methacrylate mixture followed by carbonization to remove polymethyl methacrylate and create pores in the fiber walls[176]. Sulfur was introduced by precipitation from aqueous solution with further heat treatment at 155 °C and 160 °C to infiltrate sulfur and remove any excess that is present on the surface. At low rates (0.05C), using a viscous electrolyte comprised of an ionic liquid (N-butyl-N-methylpyridinium TFSI) and PEGDME, the CNF/sulfur composite (42 wt% sulfur) exhibited an initial discharge capacity of nearly 1400 mA h $g^{-1}$ sulfur and retained 82% capacity after 30 cycles. CNF networks have also been synthesized through a templating method using an AAO membrane similar to the previous DCNT's[177]. The premise for the study was to obtain a material with sulfur residing only in the interior of the fibers so that polysulfide diffusion was limited to the ends of the fibers. This was accomplished by coating the cylindrical pores of an AAO membrane with carbonized polystyrene and subsequently infiltrating the carbon pores with sulfur. The AAO template was removed with phosphoric acid, which left CN's with only sulfur in the interior. Upon cycling the material in a low viscosity organic electrolyte it showed signs of polysulfide dissolution, with an ~ 50% capacity fade over 150 cycles at a C/5 rate, although a specific capacity of about 730 mAh $g^{-1}$ sulfur was still retained. Active mass loss may be attributable to the less than ideal sulfur confinement with such large pore substrates, but architectural improvements will undoubtedly be forthcoming soon.

3.4.4. Tubular Porous Polymers

Porous polymers have also been researched as hosts for sulfur which mimic the structure of carbon nanotubes/fibers [178-179]. Liu et al. have performed interesting studies using polyaniline nanotubes to host sulfur both in its elemental form and as part of the polymer backbone [180]. Sulfur was reacted with polyaniline nanotubes at 280 °C in order to chemically incorporate sulfur carbon bonds in the polymer through an in situ vulcanization as shown in Figure 10. Elemental sulfur was still present in the sample (62 wt%) and was postulated to be present in the pores of the polymer structure. The composite exhibited an initial capacity of 755 mAh $g^{-1}$ sulfur at a C/10 rate but the capacity increased in the next few cycles before suffering a slight capacity fade to 837 mAh $g^{-1}$ sulfur after 100 cycles. The increase in capacity was reasoned to be due to low surface area of the composite that initially did not allow electrolyte to penetrate the full structure. Upon cycling, some of the sulfur is reduced to soluble polysulfides so the additional porosity allows for higher accessibility and capacity. The capacity fading may be due to degradation of the polymersulfur backbone as the disulfide bonds in the polymer may not reform upon oxidation.

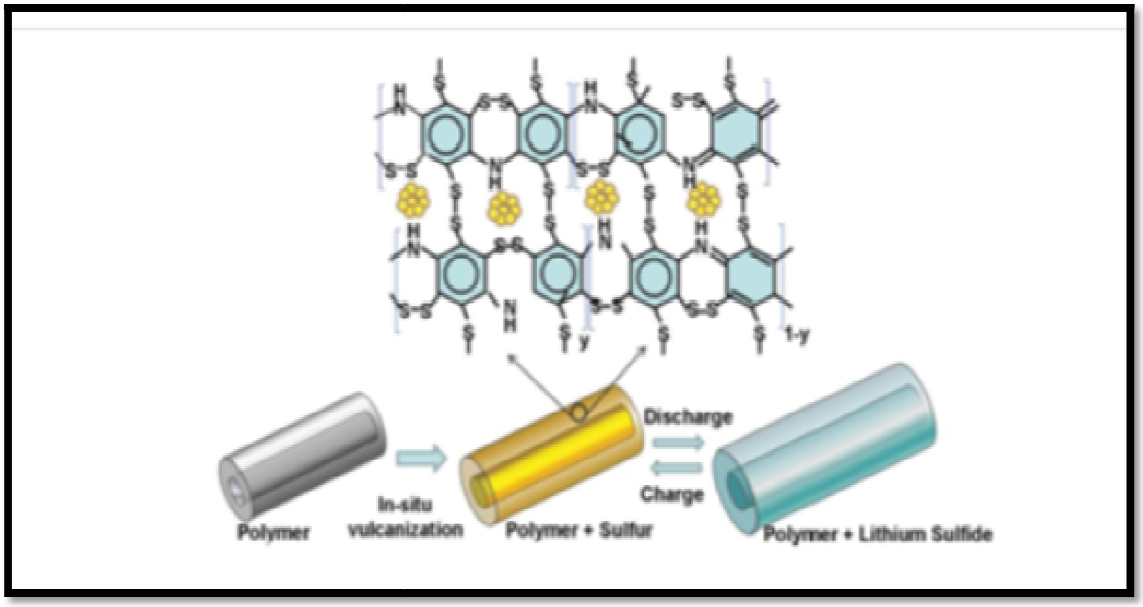



*Figure 11: Schematic Illustration of the Construction and Discharge/Charge Process of the Polyacrylonitrile Nanotube/Sulfur Composite [180].*

MWCNT's have also been used as a support to create a porous polyacrylonitrile/sulfur composite[178]. Polyacrylonitrile was coated on the exterior surface of MWCNT's and the material was treated with varying amounts of sulfur (30, 48 and 63 wt%). The best overall results were obtained for the 48 wt% sulfur composite, which exhibited 85% capacity retention, amounting to ~590 mA h $g^{-1}$ sulfur after 50 cycles at a C/10 rate. The composite has good rate capabilities and is able to be discharged up to 4C while maintaining a discharge capacity above 400 mA h $g^{-1}$ sulfur, but the average discharge voltage is low at 1.8 V and when coupled to the marginal capacity, significantly hinders the gravimetric energy density of the material.

3.4.5. Porous Metal Oxides

Carbonaceous materials are not the only hosts for sulfur that have been researched in the past few years for the Li-S battery. Tarascon et al. have taken guidance from approaches to carbon coat $LiFePO_4$ to overcome its insulating nature, by carbon coating an insulating host that serves to contain the sulfur. **[**179]. Their work utilized an insulating metalorganic framework (MIL-100) consisting of an open framework of small mesopores (~2.5- 2.9 nm) and micropores (~0.5 and ~0.9 nm). Sulfur was impregnated through the well-known melt diffusion technique, [175] affording a composite with 48 wt% sulfur. Since MIL100 is insulating, up to 50 wt% carbon was necessary to coat the particles to ensure good electrical conductivity. The material (amounting to 24 wt% sulfur in the electrode) was compared to an electrode containing mesoporous carbon CMK-3 with similar sulfur filling (52 wt%) and 20 wt% Ketjen Black (total 42 wt% sulfur in the electrode). The MIL100/S composites exhibited high capacity, and also more stable cycling, suggesting that the oxidic framework helps to retain polysulfide. This concept, using oxide additives, has a similar effect to that reported by other researchers and discussed below. The drawback is the low overall capacity of the MIL-100/S after 50 cycles at C/10 (~500 mAh $g^{-1}$ sulfur) and the low sulfur content which makes the system less practical.

**4. Physical Barrier Containment**

The previous discussion overviewed work that focused on providing a host for sulfur that contains the soluble polysulfides through architectural effects combined with chemical restraints. Another method of containment is to apply coatings to the sulfur host structure that physically blocks polysulfides from escaping the positive electrode, while still allowing ingress of the electrolyte to the sulfur/carbon mass.

*4.1. Polymer Coatings*

In the recent literature, a variety of different approaches have been utilized in order to limit polysulfide dissolution with the use of polymer coatings. Zhao et al. circumvented the use of a host material for sulfur and simply coated sulfur particles with a conducting polymer, polythiophene[180]. They were able to synthesize a polythiophene/sulfur composite with ~72 wt% sulfur that performed extremely well electrochemically. Using a low viscosity electrolyte of DOL:DME, the composite was cycled at a current density of 100 mAh $g^{-1}$ and retained 74% of its initial capacity (1120 mAh $g^{-1}$ sulfur) after 80 cycles. Cui et al. have used a carbon host (CMK-3), that is highly effective at retaining polysulfides itself because of its small ~3-4 nm pores[157] as a substrate to polymer coat in order to limit polysulfide dissolution even further as shown in Fig.11. [181]. CMK-3/S composites were prepared and mixed with the conductive polymer PEDOT:PSS which forms a thin 10-20 nm coating. While the effect of the polymer coating on electrochemical performance was not considerable, a slight increase in capacity stability was observed over bare CMK-3/S.

The PEDOT:PSS coated CMK-3/S was able to retain an overall capacity greater than 600 mAh $g^{-1}$ sulfur after 150 cycles at a C/5 rate.

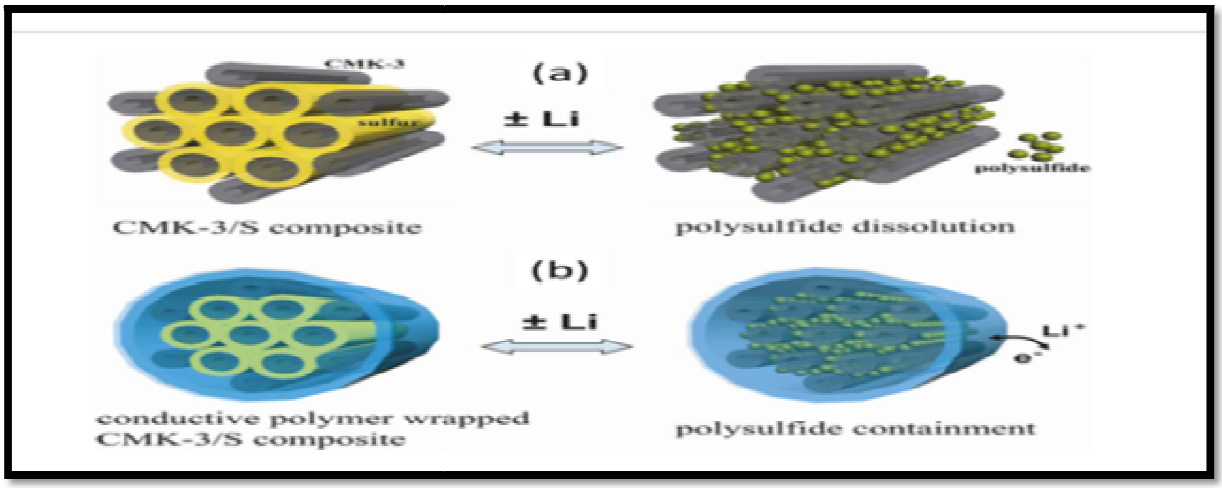



*Figure 12: Scheme of Polymer- Coated Cmk-3/ Sulfur Composite for Improving the Positive Electrode Performance, (A) in Bare CMK-3/S Particles (Gray: CMK-3, Yellow: Sulfur), Polysulfides (Green Color) Still Diffuse Out of the Carbon Matrix During Lithiation / Delithiation, (B) withConductive Polymer Coating Layer (Blue Color), Polysulfides Could Be Confined Within Carbon Matrix. Lithium Ions and Electronscan Move through This Polymer Layer [181].*

A third conducting polymer - polyaniline - has also been utilized as a coating for a MWCNT/S composite[182].The MWCNT's were impregnated with sulfur before oxidative polymerization of polyaniline. The sulfur content remained high in the composite at 70 wt% and also retained a crystalline structure. The material showed very stable cycling over 80 cycles and not surprisingly had less capacity fade than uncoated MWCNT/S. The rate capability of the material was also found to be quite good with ~90% capacity retention after 80 cycles at current densities ranging from 200 – 1000 mA $g^{-1}$ sulfur[153].

*4.2. Porous Metal Oxides*

Containing soluble polysulfides has been discussed through both physical and chemical barriers of the host material or coatings on the host material for sulfur. Another method of containment at the positive electrode is to provide additives in the positive electrode matrix that can attract and hold polysulfides so that they do not diffuse to the negative electrode. To employ this concept Nazar et al. utilized mesoporous silica as an additive to a large pore mesoporous carbon/sulfur electrode (Figure 12a)[183]. The main interaction that the polysulfides have with the additive is through surface sorption and therefore the surface area is increased significantly by synthesizing the additive with a mesoporous structure. At a C/5 rate, the capacity versus a cell without additive was both increased and much more stable over 40 cycles. The silica additive was able to sorb polysulfides during intermediate discharge and release them near the end of discharge so that they could be further reduced in the mesoporous carbon with ~94% of the sulfur being reversibly sorbed in the silica at the 40$^{th}$ cycle. The amount of sulfur present in the electrolyte after 30 cycles decreased by more than 30% compared to a cell consisting of no silica additive (Figure 12b).

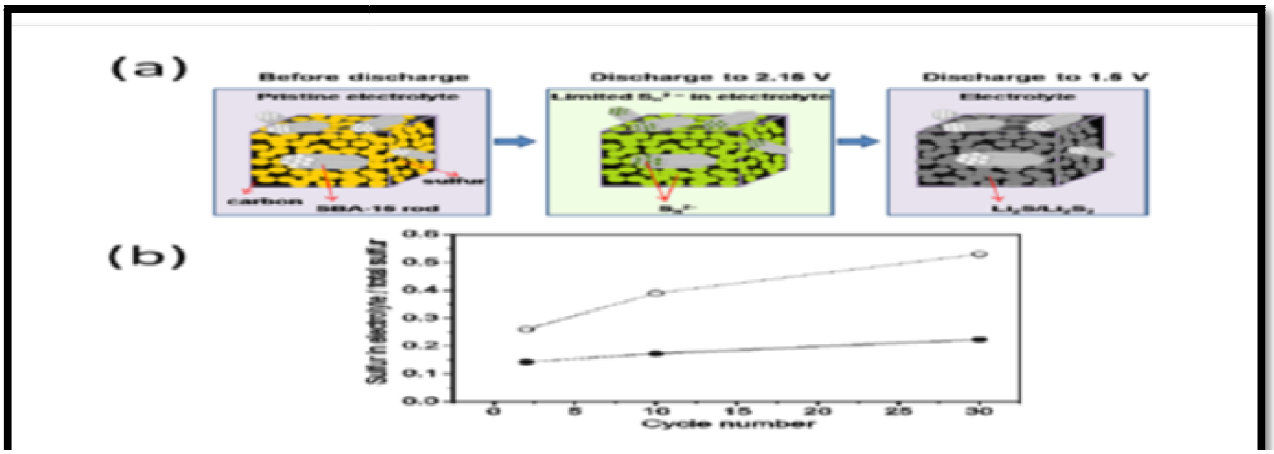



*Figure 13: A) Schematic Diagram Showing the Effect of SBA-15 Rods in the Electrode on Reversibility Absorbing/Desorbing Polysulfide Anions, B) Percentage of Sulfur Dissolution into the Electrolyte, from theSCM/S Positive Electrode (Open Dot Curve) and from the SBA -15 Added SCM/S Positive Electrode (Solid Dot Curve) [183]*

*4.3. IntercalationCathode Materials*

An intercalation cathode is a solid host network, which can store guest ions. The guest ions can be inserted into and be removed from the host network reversibly. In a Li-ion battery, $Li^+$ is the guest ion and the host network compounds are metal chalcogenides, transition metal oxides, and polyanion compounds. These intercalation compounds can be divided into several crystal structures, such as layered, spinel, olivine, and tavorite (Figure 13). The layered structure is the earliest form of intercalation compounds for the cathode materials in Li-ion batteries. Metal chalcogenides including $TiS_3$ and $NbSe_3$ were studied long ago as a possible intercalating cathode materials [184]. While $TiS_3$ exhibited only partial reversibility due to irreversible structure change from trigonal prismatic to octahedral coordination on lithiation, $NbSe_3$ demonstrated reversible electrochemical behavior. Among many different types of chalcogenides, $LiTiS_2$ (LTS) was widely studied due to its high gravimetric energy density combined with long cycle life (1000+ cycles) and was eventually commercialized by Exxon [185,186]. However, most current intercalation cathode research is focused on the transition metal oxide and polyanion compounds due to their higher operating voltage and the resulting higher energy storage capability. Typically, intercalation cathodes have 100–200 mAh/g specific capacity and 3–5 V average voltage vs. $Li/Li^+$(Figure 13e, Table 2).

| Crystal Structure | Compound | Specific Capacity ($mAh\ G^{-1}$) (Theoretical/Experi-mental/Typical In Commercial Cells) | Volumetric Capacity ($mAh\ Cm^{-3}$) (Theoretical/Typical In Commercial Cells) | Average Voltage (V) | Level Of Development |
|---|---|---|---|---|---|
| Layered | $LiTiS_2$ | 225/210 | 697 | 1.9 | Commercialized |
| | $LiCoO_2$ | 274/148/145 | 1363/550 | 3.8 | Commercialized |
| | $LiNiO_2$ | 275/150 | 1280 | 3.8 | Research |
| | $LiMnO_2$ | 285/140 | 1148 | 3.3 | Research |
| | $LiNi_{0.33}Mn_{0.33}Co_{0.33}O_2$ | 280/160/170 | 1333/600 | 3.7 | Commercialized |
| | $LiNi_{0.8}Co_{0.15}Al_{0.05}O_2$ | 279/199/200 | 1284/700 | 3.7 | Commercialized |
| | $LiMnO_3$ | 458/180 | 1708 | 3.8 | Research |
| Spinel | $LiMn2O_4$ | 148/120 | 596 | 4.1 | Commercialized |
| | $LiCo_2O_4$ | 142/84 | 704 | 4.0 | Research |
| Olivine | $LiFePO_4$ | 170/165 | 589 | 3.4 | Commercialized |
| | $LiMnPO_4$ | 171/168 | 567 | 3.8 | Research |
| | $LiCoPO_4$ | 167/125 | 510 | 4.2 | Research |
| Tavorite | $LiFeSO_4F$ | 151/120 | 487 | 3.7 | Research |
| | $LiVPO_4F$ | 156/129 | 484 | 4.2 | Research |

*Table 2: Characteristics of Representative Intercalation Cathode Compounds; Crystal Structure, Theoretical/Experimental/Commercial Gravimetric Capacities, Average Potentials, and Level of Development [184-245]*

4.3.1. TransitionMetal Oxide

$LiCoO_2$ (LCO) introduced by Goodenough [187] is the first and the most commercially successful form of layered transition metal oxide cathodes. It was originally commercialized by SONY, and this material is still used in the majority of commercial Li-ion batteries and Li-ion sulfur batteries. The Co and Li, located in octahedral sites occupy alternating layers and form a hexagonal symmetry (Fig. 13a). LCO is a very attractive cathode material because of its relatively high theoretical specific capacity of 274 mAh $g^{-1}$, high theoretical volumetric capacity of 1363 mAh $cm^{-3}$, low self-discharge, high discharge voltage, and good cycling performance [188,189]. The major limitations are high cost, low thermal stability, and fast capacity fade at high current rates or during deep cycling. LCO cathodes are expensive because of the high cost of Co (Figure 1). Low thermal stability refers to exothermic release of oxygen when a lithium metal oxide cathode is heated above a certain point, resulting in a runaway reaction in which the cell can burst into flames [190]. Thermal runaway is a major concern in the application of Li-ion batteries, resulting, for example, in the grounding of all Boeing 787 airplanes in 2013 [191]. While this issue is general to transition metal oxide intercalation cathodes, LCO has the lowest thermal stability of any commercial cathode material [192]. Although thermal stability is also largely dependent on non-materials factors such as cell design and cell size, LCO typically experiences thermal runaway past 2008C due to an exothermic reaction between the released oxygen and organic materials. Deep cycling (delithiation above 4.2 V, meaning approximately 50% or more Li extraction) induces lattice distortion from hexagonal to monoclinic symmetry and this change deteriorates cycling performance[193]. Many different types of metals (Mn, Al, Fe, Cr) [194–197] were studied as dopants/partial substitutes for Co and demonstrated promising but limited performance. Coatings of various metal oxides ($Al_2O_3$, $B_2O_3$, $TiO_2$, $ZrO_2$) [198,199] were more effective in enhancing LCO stability and performance characteristics even during deep cycling, because mechanically and chemically stable oxide material could reduce structural change of LCO and side reactions with electrolyte. $LiNiO_2$ (LNO) has same crystal structure with $LiCoO_2$ and a similar theoretical specific

capacity of 275 mAh $g^{-1}$. Its relatively high energy density and lower cost compared to Co based materials are the main research driving forces. However, pure LNO cathodes are not favorable because the $Ni^{+2}$ions have a tendency to substitute $Li^{+}$ sites during synthesis and delithiation, blocking the Li diffusion pathways [200]. LNO is also even more thermally unstable than LCO because $Ni^{+3}$ is more readily reduced than $Co^{+3}$[201]. Partial substitution of Ni with Co was found to be an effective way to reduce cationic disorder [202]. Insufficient thermal stability at high state-of-charge (SOC) can be improved via Mg doping [203], and adding a small amount of Al can improve both thermal stability and electrochemical performance [204]. As a result, the $LiNi_{0.8}Co_{0.15}Al_{0.05}O_2$ (NCA) cathode has found relatively widespread commercial use, for example, in Panasonic batteries for Tesla EVs. NCA has high usable discharge capacity (200 mAh $g^{-1}$) and long storage calendar life compared to conventional Co-based oxide cathode. However, it was reported that capacity fade may be severe at elevated temperature (40–70°C) due to solid electrolyte interface (SEI) growth and micro-crack growth at grain boundaries [205,206]. $LiMnO_2$ (LMO) can also be promising because Mn is much cheaper and less toxic compare to Co or Ni. Anhydrous and stoichiometric layered LMO was prepared almost two decades ago [207], improving on a previous aqueous methods which induced impurities, different stoichiometries, poor crystallinity, and undesirable structure change during cycling [208]. However, the cycling performance of LMO was still not satisfactory (i) because the layered structure has a tendency to change into spinel structure during Li ion extraction [208] and (ii) because Mn leaches out of LMO during cycling [209]. Mn dissolution occurs when $Mn^{+3}$ ions undergo a disproportionation reaction to form $Mn^{+2}$ and $Mn^{+4}$, and this process is observed for all cathodes containing Mn. $Mn^{+2}$ is thought to be soluble in the electrolyte, and destabilize the anode SEI. Indeed, Mn concentration in the electrolyte and anode SEI has been observed to increase with aging for Mn containing cathodes [210–213]. Also, the anode impedance is seen to increase with Mn dissolution on carbon anodes [212], but not LTO [214] (which has a negligible SEI). Stabilization of LMO via cationic doping was conducted both experimentally and theoretically [215,216], but even so, the poor cycle stability of LMO (especially at elevated temperatures) has hindered widespread commercialization. Continuous research efforts on developing cathode material less expensive than LCO resulted in the formulation of the Li $(Ni_{0.5}Mn_{0.5})O_2$ (NMO) cathode. NMO could be an attractive material because it can maintain similar energy density to LCO, while reducing cost by using lower cost transition metals. The presence of Ni allows higher Li extraction capacity to be achieved. However, cation mixing can cause low Li diffusivity and may result in unappealing rate capability [217]. Recent abinitio computational modeling predicted that low valence transition metal cations ($Ni^{+2}$) provides high-rate pathways and low strain, which are the crucial factors to achieve high rate capability in layered cathodes. NMO recently synthesized by ion exchange method showed a very low concentration of defects in NMO and capacity as high as 180 mAh $g^{-1}$even at a very high rate of 6C [218]. Adding Co into Li $(Ni_{0.5}Mn_{0.5})O_2$ was found to be effective way to enhance the structure stability further [219]. $LiNi_xCo_yMn_zO_2$ (NCM, aka NMC) has similar or higher achievable specific capacity than LCO and similar operating voltage while having lower cost since the Co content is reduced. $LiNi_{0.33}Co_{0.33}Mn_{0.33}O_2$ is the common form of NMC and is widely used in the battery market. Some of the recent efforts, such as formation of macroporous NMC, showed reversible specific capacity as high as 234 mAh $g^{-1}$and good cycle stability even at 50°C [220]. $Li_2MnO_3$ stabilized $LiMO_2$ (where M = Mn, Ni, Co) can also achieve high capacity (>200 mAh $g^{-1}$) under high voltage operation (4.5–3.0 V) [221]. $Li_2MnO_3$ is activated at >4.5 V, releasing $Li_2O$ [222] on the initial cycle which provides extra $Li^{+}$. The remaining $Li_2MnO_3$ can also facilitate Li diffusion and also act as a Li reservoir. This material group is called a lithium-rich layered oxide compound due to its extra Li ion compared to the common layered structure. More recently, novel cathode material with average composition of $LiNi_{0.68}Co_{0.18}Mn_{0.18}O_2$, in which each particle consists of bulk material surrounded by a concentration-gradient outer layer was reported [223]. The bulk material is a nickel-rich layered oxide ($LiNi_{0.8}Co_{0.1}Mn_{0.1}O_2$) for higher energy/power density (higher Ni content allows for higher Li extraction without structure deterioration), while the outer layer is Mn and Co substituted NMC($LiNi_{0.46}Co_{0.23}Mn_{0.31}O_2$) for better cycle life and safety. It is proposed that the stability of this material could originate from stable $Mn^{+4}$ in the surface layer, hence the gas evolution due to reaction between Ni ion and electrolyte is delayed. Spinel $Li_2Mn_2O_4$ (also LMO) [224] benefits from the abundance, cost, and environmental friendliness of Mn. Li occupies tetrahedral 8a sites and Mn is located in octahedral 16d sites in a ccp array of oxygen anions (Figure13b). $Li^{+}$ can diffuse through vacant tetrahedral and octahedral interstitial sites in the three-dimensional structure. The insufficient long-term cyclability is believed to originate from irreversible side reactions with electrolyte, oxygen loss from the delithiated $LiMn_2O_4$, Mn dissolution, and formation of tetragonal $Li_2Mn_2O_4$ at the surface especially at the fast c-rates [225,226]. By using nanoparticles, the rate performance can be greatly improved due to shorter $Li^{+}$diffusion lengths and improved electronic transport. Many different groups have synthesized LMO nanowires and mesoporous LMO, which show promising results [227–231]. Although decreased diffusion lengths also exacerbates the dissolution problem, it can be repressed with a surface coating of ZnO [232], Mn-rich layered structure [233], metal doping [234], oxygen stoichiometry [235], blending with different cathode materials [236], and forming a stable cathode SEI layer [237,238]. Recently, a novel ordered mesoporous lithium rich $Li_{1.12}Mn_{1.88}O_4$ spinel was demonstrated to improved electrochemical performance compare to bulk spinel [239].

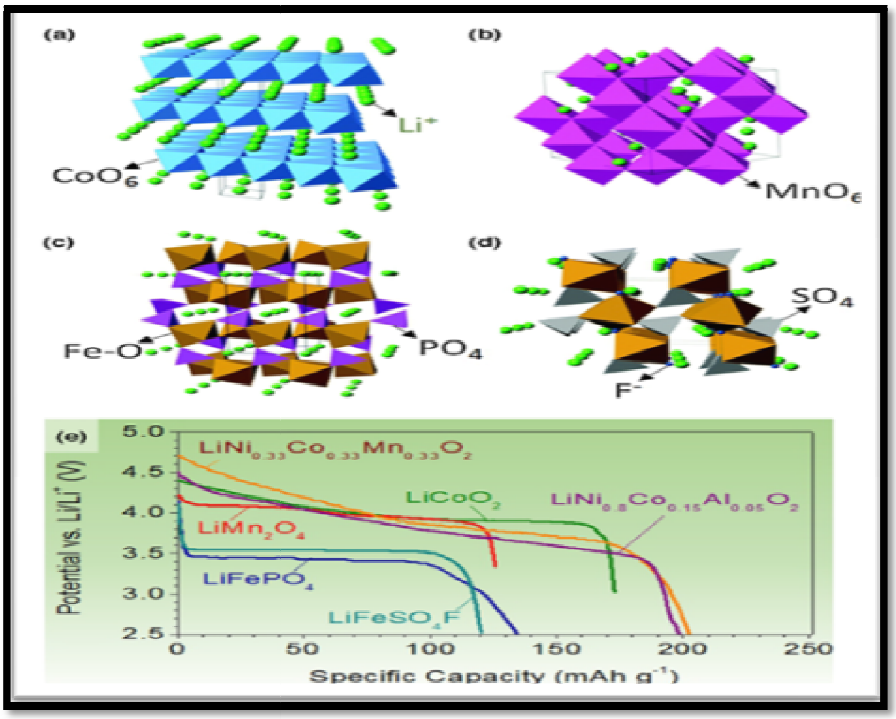



*Figure 14: Crystal Structures and Discharge Profiles of Representative Intercalation Cathodes: Structures of (A) Layered $LiCoO_2$ (B) Spinel ($LiMn_2O_4$), (C) Olivine ($LiFePO_4$), and (D) Tavorite ($LiFeSO_4F$) (Reproduced with Permission Copyright (2014) Royal Society of Chemistry) and (E) Typical Profiles of Intercalation Cathodes [240-245].*

4.3.2. Polyanion Compounds

In exploring new cathode materials, researchers have developed a new class of compounds called polyanions. Large $(XO_4)_3$_ (X = S, P, Si, As, Mo, W) polyanions occupy lattice positions and increase cathode redox potential while also stabilizing its structure [246]. $LiFePO_4$ (LFP) is the representative material for the olivine structure, known for its thermal stability and high power capability. In LFP, $Li^+$and $Fe^{+2}$occupy octahedral sites, while P is located in tetrahedral sites in a slightly distorted hexagonal close-packed (HCP) oxygen array (Figure 13c). The major weaknesses of the $LiFePO_4$ cathode include its relatively low average potential (Figure13e, Table 2) and low electrical and ionic conductivity. Intensive research over the last decade resulted in significant improvements in both performance and mechanistic understanding of LFP. Reduction in particle size in combination with carbon coating [247] and cationic doping [248] were found to be effective in increasing the rate performance. It is noteworthy that good electrochemical performance can also be achieved without carbon coating if particles are uniformly nano-sized and conductive nanocarbons are used with-in the cathodes [249]. Virus-templated amorphous anhydrous FP/ CNT composite, for example, demonstrated promising results [250]. It was reported that the facile redox reaction in non-conducting LFP could be due to a curved one-dimensional lithium diffusion path through the [0 1 0] direction [251]. In general, however, the low density of nanostructured LFP electrodes and their low average potential limit the energy density of LFP cells. Recently, a novel non-olivine allaudite LFP was reported and showed fundamentally different electrochemical behavior from that of olivine LFP [252]. Other olivine structures include $LiMnPO_4$ (LMP) which offers ~0.4 V higher average voltage compared to olivine LFP (Table 2), leading to higher specific energy, but at the expense of lower conductivity [253]. $LiCoPO_4$, $LiNi_{0.5}Co_{0.5}PO_4$, and $LiMn_{0.33}Fe_{0.33}$-$Co_{0.33}PO_4$ (LCP, NCP, MFCP) have also been developed and shown promising results, but further improvements in power, stability and energy density are required [254–256]. Novel $Li_3V_2$ $(PO_4)_3$ (LVP) exhibited relatively high operating voltage (4.0 V) and good capacity (197 mAh/g) [257]. Quite remarkably, LVP/C nanocomposite exhibited 95% theoretical capacity at a high rate of 5 C in spite of the low electronic conductivity of LVP (similar with LFP). $LiFeSO_4F$ (LFSF) is yet another interesting cathode material because of its high cell voltage and reasonable specific capacity (151 mAh $g^{-1}$) [258]. Fortunately $LiFeSO_4F$ has better ionic/electronic conductivity hence it does not desperately need carbon coating and/or nanoparticles. $LiFeSO_4F$ can also be economical since it can be prepared with abundant resources. $LiFeSO_4F$ is composed of two slightly distorted $Fe^{2+}O_4F_2$ oxyfluoride octahedra connected by F vertices in the trans position, forming chains along the c-axis, and the $Li^+$are located along the (1 0 0), (0 1 0), and (1 0 1) directions (Figure 4d). Tavorite-structured cathode materials were evaluated via simulation and reported that the fluorosulfate and fluorophosphate families of materials are the most promising and the oxysulfate family is the least [259]. The tavorite structured materials with 1D diffusion channels were suggested to exhibit low activation energies, allowing charge and discharge of Fe $(SO_4)F$ and V $(PO_4)F$ at very high rates, comparable to those observed in small olivine Fe $(PO_4)$ particles. The vanadium-containing material, LiV-$PO_4F$, cycles well, and has high voltage and capacity [260] but raise concerns about toxicity and environmental impact. Interestingly, $Li^+$ can be intercalated at ~1.8 V hence this material is able to be used in both anode ($Li^{1+x}VPO_4$ where x = 0–1) and cathode ($Li^{1-x}VPO_4$ where x = 0–1). For further detailed information on synthesis method, chemical properties and

4.3.3. Conversion Cathode Materials

Conversion electrodes undergo a solid-state redox reaction during lithiation/delithiation, in which there is a change in the crystalline structure, accompanied by the breaking and recombining chemical bonds. The full reversible electrochemical reaction for conversion electrode materials is generally as follows:

Type A $M X_z + y\ LiM + z\ Li_{(y/z)}X$ (1)

Type B $y\ Li + X\ Li_yX$ (2)

For cathodes, the Type A category (Eq. (1)) includes metal halides comprising high (2 or more) valence metal ions to give higher theoretical capacities. Figure 14a [263] shows how this reaction takes place for $FeF_2$ particles. The F ions, having the higher mobility, diffuse out of the $FeF_2$, and form LiF while nanosized phases of Fe form behind it [264]. This results in metal nanoparticles scattered in a 'sea' of the LiF ($Li_{(y/z)}X$ from Eq. (1)). The same mechanism can be more or less observed for all Type A active materials, although an intermediate Li insertion phase can also form for some. S, Se, Te, and I follow the Type B reaction (Eq. (2)). Of these elements, S has been studied the most because of its high theoretical specific capacity (1675 mAh $g^{-1}$), low cost, and abundance in the Earth's crust. Oxygen is also a Type B cathode in lithium air batteries, but poses fundamentally different technological hurdles because it is a gas. Attempts to use ambient air further complicate the issue at a systems level. Lithium air batteries are therefore not covered in this review. Figure 5b shows the intermediate steps for the full S conversion reaction, which involves intermediate polysulfides soluble in organic electrolytes. Figure 5c shows the typical discharge curves of conversion cathodes. $BiF_3$[265] and $CuF_2$[266] show promising discharge profiles with high voltage plateaus. In comparison, $Li_2S$ [267], S [268] and Se [269] also show very flat and long voltage plateaus, indicating good kinetics of the reaction between two solid phases.

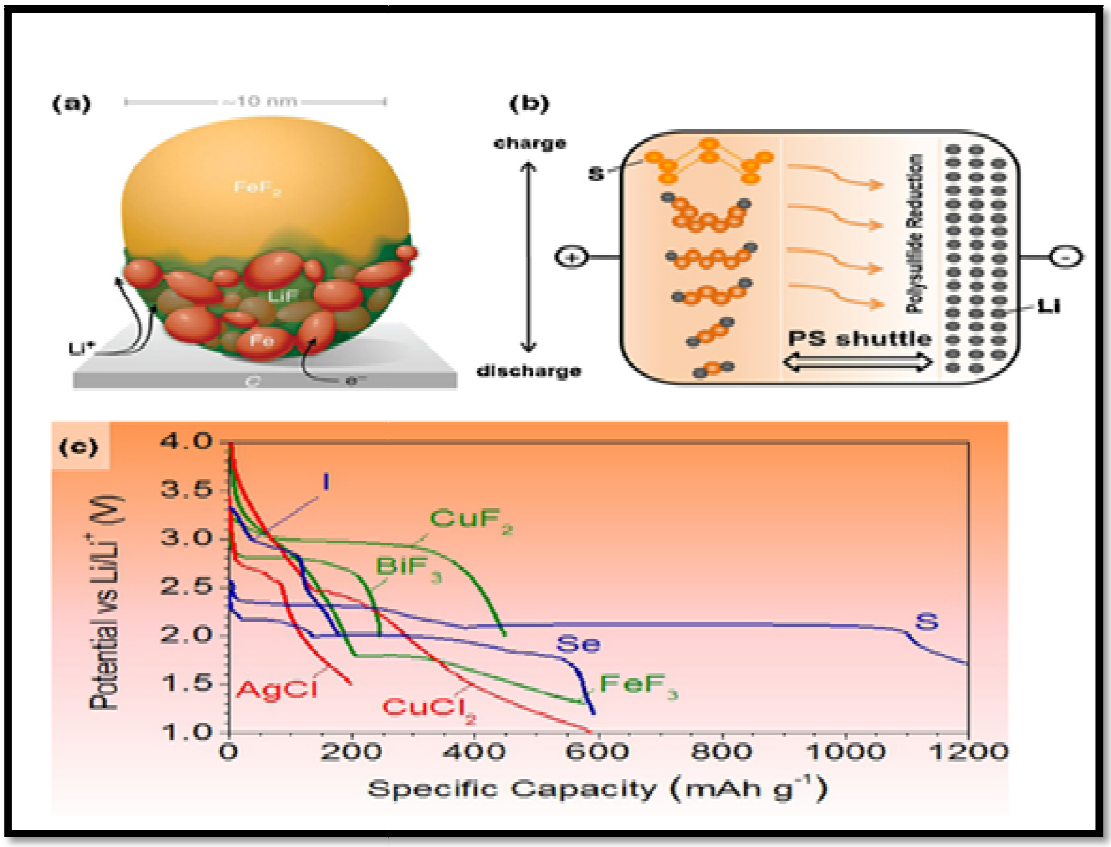



*Figure15: Transformations Accompanying Selected Conversion-Type Cathodes: (A) Propagation of Lithiation Reaction front through a Single $FeF_2$ Particle [263] (Reproduced with Copyright (2014) from Nature Publishing Group); (B) Polysulfides Shuttle Accompanyingcharge and Discharge of A S Particle and [270] and (C) Typical Discharge Profiles of Conversion Cathodes [265,266,268,271-274]*

4.3.4. Fluorine and Chlorine Compounds

Metal fluorides (MF) and chlorides (MCl) have recently been actively pursued due to intermediate operation voltages and high theoretical specific and volumetric capacities. However, MF and MCl generally suffer from poor conductivity, large voltage hysteresis, volume expansion, unwanted side reactions, and dissolution of active material (Table 3). Most MF, including $FeF_3$ and $FeF_2$, are notorious for their poor electronic conductivity because of the large band gap induced by the highly ionic character of the metal-halogen bond. However their open structures can support good ionic conduction [275,276]. Chlorides also suffer from poor electronic conductivity for the same reason. All of the reported

(Table 3) [277]. Additionally, Type A conversion materials form metal nanoparticles at their fully lithiated state. $BiF_3$ and $FeF_2$ have been reported to catalyze the decomposition of cyclic carbonates at relatively high voltages, reducing cycle life [248,278]. On the other hand, Cu nanoparticles can be electrochemically converted to $Cu^{+1}$, which then dissolves into the electrolyte [279]. Even if such unwanted side reactions do not occur, metal nanoparticles may coalesce over the course of many cycles, exacerbating the voltage hysteresis [280]. Many ionic compounds are soluble in polar solvents, and this is true for some fluorides as well [281]. Metal chlorides (including LiCl) are even more susceptible to dissolution in various solvents, including those that are used in Li battery electrolytes [282]. Meanwhile, the volume expansions of MF and MCl, as calculated by using room temperature densities of compounds before and after lithiation [283], are somewhat moderate (Table 3). The most widely studied MF and MCl materials exhibit volume expansions of 2–25%.In order to overcome their low conductivities, synthesis of nanoparticles of conversion materials is essential to shortening the pathway for the electrons and ions. For MF and MCl, active materials are often dispersed onto or wrapped in some conductive matrix materials to prepare composites with improved conductivity, such as $FeF_3$/CNT[284], $FeF_3$/grapheme[285,286], AgCl/acetylene black[272] and $BiF_3/MoS_2$/CNT [279]. Electrolyte modifications are also important [248] to minimize unfavorable reactions between the electrolyte and active material during various stages of charge and discharge.

| Materials | Electronic Conductivity (S $M^{-1}$) | Theoretical Potential (V) | Volume Expansion Fraction (%) | Voltage Hysteresis V (Vs. Li) | Qualitative Solubility in Organic Electrolytes |
|---|---|---|---|---|---|
| $FeF_2$ | insulator | 2.66 | 16.7 | 0.7-1 | - |
| $Fef_3$ | insulator | 2.74 | 25.6 | 0.8-1.6 | - |
| $CoF_2$ | Poor | 2.85 | 21 | 0.8-1.2 | Soluble |
| $CuF_2$ | Insulator | 3.55 | 11.6 | 0.8 | - |
| $NiF_2$ | Poor | 2.96 | 28.3 | 0.8-2 | - |
| $BiF_2$ | Poor | 3.18 | 1.76 | 0.5-0.7 | - |
| $FeCl_3$ | Poor | 2.83 | 22.6 | - | Soluble |
| $FeCl_2$ | Poor | 2.41 | 19.9 | - | Soluble |
| $CoCl_2$ | Poor | 2.59 | 23 | 1 | Soluble |
| $NiCl_2$ | Poor | 2.64 | 30.3 | - | Soluble |
| $CuCl_2$ | Poor | 3.07 | 21.1 | 1.2 | Soluble |
| AgCl | Poor | 2.85 | 19.4 | 0.25 | insoluble |
| LiCl | Poor | - | - | - | Soluble |
| S | Insulator $5\times10^{-30}$ | 2.38 | 79 | 0.12-0.40 | Soluble Intermediates |
| $Li_2Se$ | Insulator | 2.38 | - | 0.12-0.4 | Soluble Intermediates |
| Se | Semiconductor | 2.28 | 82.5 | 0.2-2 | Soluble Intermediates |
| $Li_2Se$ | Poor | 2.28 | - | - | Soluble Intermediates |
| Te | Semiconductor | 1.96 | 104.7 | 0.3 | - |
| I | Poor | 3.01 | 49.3 | 0.2 | Soluble |
| Lil | Poor | 3.01 | - | - | Soluble |

*Table 3: Challenges Including Conductivity, Volume Expansion, Voltage Hysteresis and Cathode Dissolution of Conversion Cathodes [257-311]*

4.3.5. Sulfur and Lithium Sulfide

Sulfur has an extremely high theoretical capacity at 1675 mAh $g^{-1}$, while also being low cost and abundant in the Earth's crust. However, S based cathodes suffer from low potential vs. $Li/Li^+$, low electrical conductivity, dissolution of intermediate reaction products (polysulfides) in electrolyte, and (in the case of pure S) very low vaporization temperature, which induces S loss while drying the electrodes under vacuum. Sulfur also suffers from _80% volume change [287], which may destroy the electrical contact in standard carbon composite electrodes [288]. To mitigate the effects of both dissolution and volume expansion, S can be encapsulated in a hollow structure with excess internal void space. Polyvinyl pyrrolidone polymer [289], carbon [290], and $TiO_2$[291] capsules have been impregnated with sulfur by using infiltration and chemical precipitation. When tested in half cells in thin electrode configurations, these composites show cycle life sometimes approaching 1000 cycles. To avoid the negative effects of expansion, prevent S evaporation during drying, and form full cells with Li free (and thus safer) anodes, electrodes have also been fabricated in the form of $Li_2S$ [292–299]. $Li_2S$ is not easily infiltrated into a host as with S because it has a much higher melting point. However, the high solubility of $Li_2S$ in various environmentally friendly solvents (such as ethanol) can be utilized to form various $Li_2S$ based nanocomposites such as, for example, $Li_2S$ nanoparticles embedded within a conductive carbon. Because the fully lithiated $Li_2S$ does not expand any further, no void spaces are necessary. In fact, carbon-coated $Li_2S$ showed no change in morphology after 400 charge/discharge cycles. Electrolyte modification is a popular method for mitigating polysulfide dissolution (Figure4f). $LiNO_3$[300] and $P_2S_5$[301] additives were used to form good SEI on the surface of Li metal to prevent the reduction and consequent precipitation of polysulfides. Lithium polysulfides can also be added to temporarily decrease cathode

dissolution [302]. Multiple papers also utilized higher molarity electrolytes, which also greatly reduces polysulfide solubility [303,304]. Finally, solid state electrolytes can also prevent polysulfide dissolution, and at the same time, enhance cell safety by avoiding Li dendrite short circuiting [305–307].

*4.3.6. Selenium and Tellurium*

Recently, Se and Te have attracted attention due to their higher electronic conductivities than S and high theoretical volumetric capacities of 1630 mAh $cm^{-3}$and 1280 mAh $cm^{-3}$, respectively, in the fully lithiated state. Due to the higher electronic conductivity, Se and Te often show higher utilization of active materials and higher rate capability than S. Similar to S, the Se-based cathodes suffer from the dissolution of high-order polyselenides [308], resulting in fast capacity loss, poor cycle performance and low coulombic efficiency. So far, the dissolution of polytelluride has not been reported. As seen in Table 3, elemental Se and Te also suffer from large volume change. Fortunately, Se and Te are also similar to S in that they have low melting points. Both materials have been infiltrated into various porous carbon hosts [308, 309], and dispersed or wrapped in conductive matrices [310] to improve their performance. However, Te is far too expensive for practical use. Moreover, Se and Te are of similar abundance as Ag and Au (Figure 1), and are very unlikely to be used in mass production.

4.3.7. Iodine

The lithium-iodine primary battery uses LiI as a solid electrolyte ($10^{-9}$ S $cm^{-1}$), resulting in low self-discharge rate and high energy density, and is an important power source for implantable cardiac pacemaker applications. The cathodic I is first reduced into the triiodide ion ($I^{3-}$) and then into the iodide ion ($I^-$) during discharge [311]. For use in most other applications, this chemistry is problematic, however, because of its low power capability. Further-more, in standard organic electrolytes, iodine, triodide, and lithium iodide are all soluble [311]. Due to the high solubility of LiI in organic solvents, iodine ions have been considered for use in lithium-flow batteries instead. Recently, active iodine was infiltrated into the pores of porous carbon due to low melting point of I (1138˚C). The as-produced iodine–conductive carbon black composite showed a high discharge voltage plateau, good cycle performance, and high rate capability, which is attributed to the enhanced electronic conductivity and suppressed active material dissolution [311].

## 5. Conclusion

The Li-ion sulfur battery has clear fundamental advantages and decades of research which have developed it into the high energy density, high cycle life, high efficiency battery that it is today. Yet research continues on new electrode materials to push the boundaries of cost, energy density, power density, cycle life, and safety. Various promising anode and cathode materials exist, but many suffer from limited electrical conductivity, slow Li transport, dissolution or other unfavorable interactions with electrolyte, low thermal stability, high volume expansion, and mechanical brittleness.Various methods have been pursued to overcome these challenges, as summarized in **Fig. 4**. Many intercalation cathodes have been brought to market, and conversion material technology is slowly coming closer to a widespread commercialization. The last couple of decades have been an exciting time for research in the field of Li-ionsulfur battery electrode materials;especially over the last few years, but more improvements are still needed at the positive electrode. The containment of polysulfides is critical to increase cycle life and minimize capacity fading. Achieving full, reversible reduction of $Li_2S_2$ to $Li_2S$, which accounts for half of the theoretical capacity, is vital to improving energy density. Fundamental studies are necessary to understand and control this process better. As new materials and strategies are found, Li-ion sulfur batteries will no doubt have an ever greater impact on our lives in the years to come.

## 6. References


i. Z. W. Seh, Y. M. Sun, Q. F. Zhang, Y. Cui, Chem. Soc. Rev. 2016, 45, 5605- 5634.
ii. A. Rosenman, E. Markevich, G. Salitra, D. Aurbach, A. Garsuch, F. F. Chesneau, Adv. Energy Mater. 2015, 5, 1500212.
iii. J. L. Wang, Y.-S. He, J. Yang, Adv. Mater. 2015, 27, 569–575.
iv. E. M. Jin, B. Jin, D.-K. Jun, K.-H. Park, H.-B. Gu, K.-W. Kim, J. Power Sources 2008, 178, 801-806.
v. H.-C. Kang, D.-K. Jun, B. Jin, E. M. Jin, K.-H. Park, H.-B. Gu, K.-W. Kim, J. Power Sources 2008, 179, 340-346.
vi. A. Rosenman, E. Markevich, G. Salitra, D. Aurbach, A. Garsuch, F. F. Chesneau, Adv. Energy Mater. 2015, 5, 1500212.
vii. J.M. Tarascon, M. Armand, Nature 414 (6861) (2001) 359.
viii. G. Y. Xu, B. Ding, J. Pan, P. Nie, L. F. Shen, X. G. Zhang, J. Mater. Chem. A 2014, 2, 12662–12676.
ix. R. J. Chen, T. Zhao, F. Wu, Chem. Commun. 2015, 51, 18-33.
x. J. H. Yan, X. B. Liu, M. Yao, X. F. Wang, T. K. Wafle, B. Y. Li, Chem. Mater. 2015, 27, 5080–5087.
xi. M.-S. Park, B. O. Jeong, T. J. Kim, S. Kim, K. J. Kim, J.-S. Yu, Y. J. Jung, Y.-J. Kim, Carbon 2014, 68, 265-272.
xii. T. Xu, J. X. Song, M. L. Gordin, H. S. Sohn, Z. X. Yu, S. R. Chen, D. H. Wang, ACS Appl. Mater. Inter. 2013, 5, 11355-11362.
xiii. J. H. Xu, B. Jin, H. Li, Q. Jiang, Int. J. Hydrogen Energ. 2017, 42, 20749-20758.
xiv. S. S. Li, B. Jin, H. Li, C. W. Dong, B. Zhang, J. H. Xu, Q. Jiang, J. Electroanal. Chem. 2017, 806, 41-49.
xv. R. Xu, J. Lu, K. Amine, Adv. Energy Mater. 2015, 5, 1500408.
xvi. L. Ma, K. E. Hendrickson, S. Y. Wei, L. A. Archer, Nano Today 2015, 10, 315-338.
xvii. R. Xu, I. Belharouak, X. F. Zhang, R. Chamoun, C. Yu, Y. Ren, A. Nie, R. Shahbazian-Yassar, J. Lu, J. C. Li, K. Amine, ACS Appl. Mater. Inter. 2014, 6, 21938-21945.
xviii. M.-K. Song, Y. G. Zhang, E. J. Cairns, Nano Lett. 2013, 13, 5891-5899.

xix. O. Ogoke, G. Wu, X. L. Wang, A. Casimir, L. Ma, T. P. Wu, J. Lu, J. Mater. Chem. A 2017, 5, 448-469. [20] A. Manthiram, S.-H. Chung, C. X. Zu, Adv. Mater. 2015, 27, 1980-2006.
xx. L. Chen, L. L. Shaw, J. Power Sources 2014, 267, 770-783.
xxi. M.-K. Song, E. J. Cairns, Y. G. Zhang, Nanoscale 2013, 5, 2186-2204.
xxii. Z. Li, H. B. Wu, X. W. Lou, Energy Environ. Sci. 2016, 9, 3061-3070.
xxiii. D. Herbert, J. Ulam, United States Patent Office 1962, 3043896.
xxiv. A. Manthiram, Y. Z. Fu, Y.-S. Su, Acc. Chem. Res. 2013, 46, 1125-1134.
xxv. W. M. Kang, N. P. Deng, J. G. Ju, Q. X. Li, D. Y. Wu, X. M. Ma, L. Li, M. Naebe, B. W. Cheng, Nanoscale 2016, 8,16541–16588.
xxvi. S. Urbonaite, T. Poux, P. Novk, Adv. Energy Mater. 2015, 5, 1500118.
xxvii. C. Grosjean, et al. Renew. Sustain. Energy Rev. 16 (3) (2012) 1735.
xxviii. M. Lowe, et al., Lithium-ion Batteries for Electric Vehicles: The U.S. Value Chain, Center on Globalization, Governance & Competitiveness, 2010.
xxix. P.A. Nelson, et al., Modeling the Performance and Cost of Lithium-Ion Batteries for Electric-Drive Vehicles, Argonne National Laboratory, 2012.
xxx. N.N. Greenwood, A. Earnshaw, Chemistry of the Elements, 2nd ed., Butterworth-Heinemann, Burlington, MA, 1997.
xxxi. S. Moores, How is Natural Graphite Priced? Industrial Minerals, 2013.
xxxii. USGS, Minerals Information, 1932-2013.
xxxiii. Sulfur Price, National Iranian Gas Company, 2014.
xxxiv. P. Strubel, S. Thieme, T. Biemelt, A. Helmer, M. Oschatz, J. Bru¨ckner, H. Althues, S. Kaskel, Adv. Funct. Mater. 25 (2015) 287-297.
xxxv. Z. Lyu, D. Xu, L. Yang, R. Che, R. Feng, J. Zhao, Y. Li, Q. Wu, X. Wang, Z. Hu, Nano Energy 12 (2015) 657-665.
xxxvi. Y. Hou, J. Li, X. Gao, Z. Wen, C. Yuan, J. Chen, Nanoscale 8 (2016) 8228-8235.
xxxvii. C. Reitz, B. Breitung, A. Schneider, D. Wang, M.v.d. Lehr, T. Leichtweiss, J. Janek, H. Hahn, T. Brezesinski, ACS Appl. Mater. Interfaces 8 (2016) 10274-10282.
xxxviii. D.W. Xu, S. Xin, Y. You, Y. Li, H.P. Cong, S.H. Yu, ChemNanoMat 2 (2016) 712-718.
xxxix. S.K. Park, J. Lee, T. Hwang, B. Jang, Y. Piao, ACS Appl. Mater. Interfaces 9 (2017) 2430e2438.
xl. L. Yu, H. Hu, H.B. Wu, X.W. Lou, Adv. Mater. 29 (2017) 1604563.
xli. K. Zhou, X. Fan, X. Wei, J. Liu, Sci. China Tech. Sci. 60 (2017) 175-185.
xlii. G. Zhou, L.C. Yin, D.W. Wang, L. Li, S. Pei, I.R. Gentle, F. Li, H.M. Cheng, ACS Nano 7 (2013) 5367-5375. [44] C.P. Yang, Y.X. Yin, H. Ye, K.C. Jiang, J. Zhang, Y.G. Guo, ACS Appl. Mater. Interfaces 6 (2014) 8789-8795.
xliii. W. Zhou, C. Wang, Q. Zhang, H.D. Abru~na, Y. He, J. Wang, S.X. Mao, X. Xiao, Adv. Energy Mater. 5 (2015) 1401752.
xliv. R. Cao, W. Xu, D. Lv, J. Xiao, and J.-G. Zhang, Adv. Energy Mater., 5, 1402273 (2015).
xlv. H.-J. Peng, J.-Q. Huang, and Q. Zhang, Chem. Soc. Rev., 46, 5237 (2017).
xlvi. J. Lochala, D. Liu, B. Wu, C. Robinson, and J. Xiao, ACS Appl. Mater. Interfaces,9, 24407 (2017).
xlvii. J. Liu, W. Li, L. Duan, X. Li, L. Ji, Z. Geng, K. Huang, L. Lu, L. Zhou, Z. Liu, W. Chen, L. Liu, S. Feng, Y. Zhang, Nano Lett. 15 (2015) 5137-5142.
xlviii. H. Yao, G. Zheng, P.C. Hsu, D. Kong, J.J. Cha, W. Li, W.S. Zhi, M.T. Mcdowell, K. Yan, Z. Liang, Nat. Commun. 5 (2014) 3943.
xlix. S. Yuan, Z. Guo, L. Wang, S. Hu, Y. Wang, Y. Xia, Adv. Sci. 2 (2015) 1500071.
l. A. Manthiram, Y. Fu, S.H. Chung, C. Zu, Y.S. Su, Chem. Rev. 114 (2014) 11751-11787
li. S.H. Chung, R. Singhal, V. Kalra, A. Manthiram, J. Phys. Chem. Lett. 6 (2015) 2163-2169.
lii. M. Wild, L. O'Neill, T. Zhang, R. Purkayastha, G. Minton, M. Marinescu, G.J. Offer, Energy Environ. Sci. 8 (2015) 3477-3494.
liii. R. Xu, J. Lu, K. Amine, Adv. Energy Mater. 5 (2015) 1500408.
liv. M.A. Pope, I.A. Aksay, Adv. Energy Mater. 5 (2015) 1500124.
lv. Y. Yang, G. Zheng, Y. Cui, Chem. Soc. Rev. 42 (2013) 3018-3032.
lvi. J.R. Akridge, Y.V. Mikhaylik, N. White, Solid State Ionics 175 (2004) 243-245.
lvii. C. Barchasz, F. Molton, C. Duboc, J.C. Lepr^etre, S. Patoux, F. Alloin, A. Chem, Anal. Chem. 84 (2012) 3973-3980.
lviii. S. Zhang, K. Ueno, K. Dokko, M. Watanabe, Adv. Energy Mater. 5 (2015) 1500117.
lix. L. Qie, C. Zu, A. Manthiram, Adv. Energy Mater. 6 (2016) 1502459.
lx. S.H. Chung, A. Manthiram, ChemSusChem 7 (2014) 1655-1661.
lxi. R. Fang, S. Zhao, P. Hou, M. Cheng, S. Wang, H.M. Cheng, C. Liu, F. Li, Adv. Mater. 28 (2016) 3374-3382.
lxii. H. Chen, C. Wang, Y. Dai, J. Ge, W. Lu, J. Yang, L. Chen, Nano Energy 26 (2016) 43-49.
lxiii. T. Tao, S. Lu, Y. Fan, W. Lei, S. Huang, and Y. Chen, Adv. Mater., 29, 1700542 (2017).
lxiv. J.-Q. Huang, P.-Y. Zhai, H.-J. Peng, W.-C. Zhu, and Q. Zhang, Sci. Bull., 62, 1267 (2017).
lxv. Y. Liu, B. Li, S. Li, J. Liu, and S. Yang, J. Mater. Chem. A, 5, 18862 (2017).
lxvi. X.-B. Cheng, C. Yan, J.-Q. Huang, P. Li, L. Zhu, L. Zhao, Y. Zhang, W. Zhu,S.-T. Yang, and Q. Zhang, Energy Storage Mater., 6, 18 (2017).
lxvii. X. Chen, T.-Z. Hou, B. Li, C. Yan, L. Zhu, C. Guan, X.-B. Cheng, H.-J. Peng,J.-Q. Huang, and Q. Zhang, Energy Storage Mater., 8, 194 (2017).
lxviii. Y. Guo, H. Li, and T. Zhai, Adv. Mater., 29, 1700007 (2017).
lxix. B. Wu, J. Lochala, T. Taverne, and J. Xiao, Nano Energy, 40, 34 (2017).
lxx. K. N. Wood, M. Noked, and N. P. Dasgupta, ACS Energy Lett., 2, 664 (2017).

lxxi. D. Lu, Y. Shao, T. Lozano, W. D. Bennett, G. L. Graff, B. Polzin, J. Zhang, M. H. Engelhard,N. T. Saenz,W. A. Henderson, P. Bhattacharya, J. Liu, and J. Xiao,Adv. Energy Mater., 5, 1400993 (2015).
lxxii. O. O. Taiwo, D. P. Finegan, J. M. Paz-Garcia, D. S. Eastwood, A. J. Bodey, C. Rau,S. A. Hall, D. J. L. Brett, P. D. Lee, and P. R. Shearing, Phys. Chem. Chem. Phys.,19, 22111 (2017).
lxxiii. R. Zhang, X.-B. Cheng, C.-Z. Zhao, H.-J. Peng, J.-L. Shi, J.-Q. Huang, J. Wang,F. Wei, and Q. Zhang, Adv. Mater., 28, 2155 (2016).
lxxiv. S. Walu´s, G. Offer, I. Hunt, Y. Patel, T. Stockley, J. Williams, and R. Purkayastha,Energy Storage Mater., (2017).
lxxv. W. Xu, et al. Energy Environ. Sci. 7 (2) (2014) 513.
lxxvi. N.A. Kaskhedikar, J. Maier, Adv. Mater. 21 (25–26) (2009) 2664.
lxxvii. G.-N. Zhu, et al. Energy Environ. Sci. 5 (5) (2012) 6652.
lxxviii. Z. Chen, et al. Adv. Funct. Mater. 23 (8) (2013) 959.
lxxix. N. Nitta, G. Yushin, Part. Part. Syst. Charact. 31 (3) (2014) 317.
lxxx. J. Cabana, et al. Adv. Mater. 22 (35) (2010) E170.
lxxxi. C.-M. Park, et al. Chem. Soc. Rev. 39 (8) (2010) 3115.
lxxxii. D. Aurbach, et al. Electrochim. Acta 45 (1–2) (1999) 67.
lxxxiii. D. Bar-Tow, et al. J. Electrochem. Soc. 146 (3) (1999) 824.
lxxxiv. D. Billaud, et al. Mater. Res. Bull. 14 (7) (1979) 857.
lxxxv. Y. Qi, et al. J. Electrochem. Soc. 157 (5) (2010) A558.
lxxxvi. H. Nozaki, et al. J. Power Sources 194 (1) (2009) 486.
lxxxvii. Carbon Powders for Lithium Battery Systems, Timcal Graphite & Carbon, Switzerland, 2005.
lxxxviii. M. Winter, et al. Adv. Mater. 10 (10) (1998) 725.
lxxxix. R. Mukherjee, et al. Nat. Commun. (2014) 5.
xc. J.R. Dahn, et al. Science 270 (5236) (1995) 590.
xci. T. Zheng, et al. J. Electrochem. Soc. 142 (8) (1995) 2581.
xcii. D. Doughty, E.P. Rother, Electrochem. Soc. Interface 21 (2) (2012) 35.
xciii. S. Scharner, et al. J. Electrochem. Soc. 146 (3) (1999) 857.
xciv. M. Wagemaker, et al. Adv. Mater. 18 (23) (2006) 3169.
xcv. J.-F. Colin, et al. Electrochem. Commun. 12 (6) (2010) 804.
xcvi. H.-G. Jung, et al. Nat. Commun. 2 (2011) 516.
xcvii. F.X. Wu, et al. Electrochim. Acta 78 (2012) 331.
xcviii. Y.-B. He, et al. Sci. Rep. (2012) 2.
xcix. Y.-B. He, et al. J. Power Sources 239 (2013) 269.
c. M.-S. Song, et al. J. Mater. Chem. A 2 (3) (2014) 631.
ci. K. Zaghib, et al. J. Power Sources 196 (8) (2011) 3949.
cii. SCiB: Super Charge Ion battery, Toshiba.
ciii. J. Wang, et al. Angew. Chem. Int. Ed. 53 (17) (2014) 4460.
civ. C.K. Chan, et al. Nat. Nano 3 (1) (2008) 31.
cv. Y. Oumellal, et al. J. Mater. Chem. 21 (17) (2011) 6201.
cvi. A. Magasinski, et al. Nat. Mater. 9 (4) (2010) 353.
cvii. B. Hertzberg, et al. J. Am. Chem. Soc. 132 (25) (2010) 8548.
cviii. B. Wang, et al. Adv. Mater. 25 (26) (2013) 3560.
cix. N. Liu, et al. Nano Lett. 12 (6) (2012) 3315.
cx. S. Chen, et al. Phys. Chem. Chem. Phys. 14 (37) (2012) 12741.
cxi. Y. Park, et al. Adv. Energy Mater. 3 (2) (2013) 206.
cxii. H. Tao, et al. Nanoscale 6 (6) (2014) 3138.
cxiii. N. Liu, et al. Nat. Nano 9 (3) (2014) 187.
cxiv. H. Nakai, et al. J. Electrochem. Soc. 158 (7) (2011) A798.
cxv. S. Dalavi, et al. J. Electrochem. Soc. 159 (5) (2012) A642.
cxvi. A. Bordes, et al. J. Power Sources 257 (2014) 163.
cxvii. J. Li, et al. Electrochem. Solid State Lett. 10 (2) (2007) A17.
cxviii. N.S. Hochgatterer, et al. Electrochem. Solid State Lett. 11 (5) (2008) A76.
cxix. A. Magasinski, et al. ACS Appl. Mater. Interfaces 2 (11) (2010) 3004.
cxx. I. Kovalenko, et al. Science 333 (6052) (2011) 75.
cxxi. M.-H. Ryou, et al. Adv. Mater. 25 (11) (2013) 1571.
cxxii. L. Xu, et al. Nano Lett. (2013).
cxxiii. X.H. Liu, et al. Nano Lett. 11 (9) (2011) 3991.
cxxiv. W. Liang, et al. ACS Nano (2013).
cxxv. H. Okamoto, J. Phase, Equilib. Diffus. 27 (2) (2006) 200.
cxxvi. Y. Liu, et al. Nano Lett. 11 (10) (2011) 4188.
cxxvii. J. Qian, et al. Chem. Commun. 48 (71) (2012) 8931.
cxxviii. A. Darwiche, et al. J. Am. Chem. Soc. 134 (51) (2012) 20805.
cxxix. Y. Yamada, et al. ACS Appl. Mater. Interfaces (2014).
cxxx. K. Teshima, et al. Cryst. Growth Des. 11 (10) (2011) 4401.
cxxxi. M.K.Y. Chan, et al. J. Am. Chem. Soc. 134 (35) (2012) 14362.

cxxxii. T.D. Hatchard, J.R. Dahn, J. Electrochem. Soc. 151 (6) (2004) A838.
cxxxiii. K. Zhong, et al. J. Power Sources 196 (16) (2011) 6802.
cxxxiv. M.E. Spahr, in: M. Yoshio, et al. (Eds.), Lithium-Ion Batteries: Science and Technologies, Springer, 2009, pp. 117.
cxxxv. H.C. Yu, et al. Energy Environ. Sci. 7 (5) (2014) 1760.
cxxxvi. A.J. Gmitter, et al. J. Mater. Chem. 20 (20) (2010) 4149.
cxxxvii. X. Hua, et al. J. Phys. Chem. C (2014).
cxxxviii. P. Liu, et al. J. Phys. Chem. C 116 (10) (2012) 6467.
cxxxix. M.A. Reddy, et al. Adv. Energy Mater. 3 (3) (2013) 308.
cxl. R. Ma, et al. J. Mater. Chem. A 1 (47) (2013) 15060.
cxli. L. Li, et al. Nano Lett. 12 (11) (2012) 6030.
cxlii. K. Kang, et al. Science 311 (5763) (2006) 977.
cxliii. N. Yabuuchi, T. Ohzuku, J. Power Sources 119–121 (2003) 171.
cxliv. K.M. Shaju, P.G. Bruce, Adv. Mater. 18 (17) (2006) 2330.
cxlv. M.M. Thackeray, et al. J. Mater. Chem. 17 (30) (2007) 3112.
cxlvi. S. Hy, et al. J. Am. Chem. Soc. 136 (3) (2013) 999.
cxlvii. Y.-K. Sun, et al. Nat. Mater. 8 (4) (2009) 320.
cxlviii. M.M. Thackeray, Prog. Solid State Chem. 25 (1) (1997) 1.
cxlix. J. A. Dean, Lange's Handbook of Chemistry, McGraw-Hill, New York, (1985).
cl. H. Yamin and E. Peled, J. Power Sources, 9, 281, (1983).
cli. J. I. Yamaki, S. I. Tobishima, Y. Sakurai, K. I. Saito and K. Hayashi, J. Appl. Electrochem., 28, 135, (1998).
clii. S. E. Cheon, K. S. Ko, J. H. Cho, S. W. Kim, E. Y. Chin and H. T. Kim, J. Electrochem. Soc., 150, A800, (2003).
cliii. B. H. Jeon, J. H. Yeon, K. M. Kim and I. J. Chung, J. Power Sources, 109, 89, (2002).
cliv. N. Tachikawa, K. Yamauchi, E. Takashima, J. Park, K. Dokko and M. Watanabe, Chem. Commun., 47, 8157, (2011).
clv. X. Ji, K. T. Lee and L. F. Nazar, Nature Mater., 8, 500, (2009).
clvi. X. Li, Y. Cao, W. Qi, L. V. Saraf, J. Xiao, Z. Nie, J. Mietek, J. G. Zhang, B. Schwenzer and J. Liu, J. Mater. Chem., 21, 16603, (2011).
clvii. C. Liang, N. J. Dudney and J. Y. Howe, Chem. Mater., 21, 4724, (2009).
clviii. G. He, X. Ji and L. F. Nazar, Energy & Environ. Sci., 4, 2878, (2011).
clix. S. R. Chen, Y. P. Zhai, G. L. Xu, Y. X. Jiang, D. Y. Zhao, J. T. Li, L. Huang and S. G. Sun, Electrochim. Acta, 56, 9549 (2011).
clx. J. Schuster, G. He, T. Bein and L. F. Nazar, Angew. Chem., 51, 3591, (2012).
clxi. N. Jayaprakash, J. Shen, S. S. Moganty, A. Corona and L. A. Archer, Angew. Chem. Int. Ed., 50, 5904, (2011).
clxii. B. Zhang, X. Qin, G. R. Li and X. P. Gao, Energy & Environ. Sci., 3, 1531, (2010).
clxiii. J. Gao, M. A. Lowe, Y. Kiya and H. D. Abruña, J. Phys. Chem. C, **115**, 25132, (2011).
clxiv. R. Elazari, G. Salitra, A. Garsuch, A. Panchenko and D. Aurbach, Adv. Mater., **23**, 5641, (2011).
clxv. J. Z. Wang, L. Lu, M. Choucair, J. A. Stride, X. Xu and H. K. Liu, J. Power Sources, **196**, 7030, (2011).
clxvi. H. Wang, Y. Yang, Y. Liang, J. T. Robinson, Y. Li, A. Jackson, Y. Cui and H. Dai, Nano Lett., **11**, 2644, (2011).
clxvii. Y. Cao, X. Li, Aksay, J. Lemmon, Z. Nie, Z. Yang and J. Liu, Phys. Chem. Chem. Phys., **13**, 7660, (2011).
clxviii. L. Ji, M. Rao, H. Zheng, L. Zhang, Y. Li, W. Duan, J. Guo, E. J. Cairns and Y. Zhang, J. Am. Chem. Soc., **133**, 18522, (2011).
clxix. S. Evers and L. F. Nazar, Chem. Commun., **48**, 1233, (2012).
clxx. Y. X. Wang, L. Huang, L. C. Sun, S. Y. Xie, G. L. Xu, S. R. Chen, Y. F. Xu, J. T. Li, S. L. Chou, S. X. Dou and S. G. Sun, J. Mater. Chem., **22**, 4744, (2012).
clxxi. W. Ahn, K. B. Kim, K. N. Jung, K. H. Shin and C. S. Jin, J. Power Sources, **202**, 394, (2012).
clxxii. J. Guo, Y. Xu and C. Wang, Nano Lett., **11**, 4288, (2011).
clxxiii. M. Rao, X. Song and E. J. Cairns, J. Power Sources, **205**, 474, (2012).
clxxiv. L. Ji, M. Rao, S. Aloni, L. Wang, E. J. Cairns and Y. Zhang, Energy Environ. Sci., **4**, 5053, (2011).
clxxv. G. Zheng, Y. Yang, J. J. Cha, S. S. Hong and Y. Cui, Nano Lett., **11**, 4462, (2011).
clxxvi. L. Yin, J. Wang, J. Yang and Y. Nuli, J. Mater. Chem., **21**, 6807, (2011).
clxxvii. R. Demir-Cakan, M. Morcette, F. Nouar, C. Davoisne, T. Devic, D. Gonbeau, R. Dominko, C. Serre, G. Férey and J. M. Tarascon, J. Am. Chem. Soc., **133**, 16154, (2011).
clxxviii. F. Wu, J. Chen, R. Chen, S. Wu, L. Li, S. Chen and T. Zhao, J. Phys. Chem. C, **115**, 6057, (2011).
clxxix. Y. Yang, G. Yu, J. J. Cha, H. Wu, M. Vosgueritchian, Y. Yao, Z. Bao and Y. Cui, ACS Nano, **5**, 9187, (2011).
clxxx. F. Wu, J. Chen, L. Li, T. Zhao and R. Chen, J. Phys. Chem. C, **115**, 24411, (2011).
clxxxi. X. Ji, S. Evers, R. Black and L. F. Nazar, Nature Commun., **2**, 325, (2011).
clxxxii. D.W. Murphy, F.A. Trumbore, J. Electrochem. Soc. 123 (7) (1976) 960.
clxxxiii. M.S. Whittingham, Science 192 (4244) (1976) 1126.
clxxxiv. M.S. Whittingham, Chem. Rev. 104 (10) (2004) 4271.
clxxxv. K. Mizushima, et al. Mater. Res. Bull. 15 (6) (1980) 783.
clxxxvi. R. Yazami, et al. New Trends in Intercalation Compounds for Energy Storage and Conversion: Proceedings of the International Symposium, The Electrochemical Society, vol. 2003, 2003, p. 317.
clxxxvii. A. Du Pasquier, et al. J. Power Sources 115 (1) (2003) 171.
clxxxviii. J.R. Dahn, et al. Solid State Ionics 69 (3–4) (1994) 265.
clxxxix. N. Williard, et al. Energies 6 (9) (2013) 4682.

cxc. D. Doughty, E.P. Rother, Electrochem. Soc. Interface 21 (2) (2012) 35.
cxci. J.N. Reimers, J. Dahn, J. Electrochem. Soc. 139 (8) (1992) 2091.
cxcii. G. Ceder, et al. Nature 392 (6677) (1998) 694.
cxciii. R. Alca´ntara, et al. J. Power Sources 81–82 (1999) 547.
cxciv. S. Madhavi, et al. Electrochim. Acta 48 (3) (2002) 219.
cxcv. R. Stoyanova, et al. Solid State Ionics 73 (3–4) (1994) 233.
cxcvi. J. Cho, et al. Angew. Chem. 113 (18) (2001) 3471.
cxcvii. I.D. Scott, et al. Nano Lett. 11 (2) (2010) 414.
cxcviii. A. Rougier, et al. J. Electrochem. Soc. 143 (4) (1996) 1168.
cxcix. H. Arai, et al. Solid State Ionics 109 (3) (1998) 295.
cc. P. Kalyani, N. Kalaiselvi, Sci. Technol. Adv. Mater. 6 (6) (2005) 689.
cci. S.L. Dalton, et al., Lithium metal oxide materials and methods of synthesis and use, Google Patents (2008).
ccii. C. Chen, et al. J. Power Sources 128 (2) (2004) 278.
cciii. I. Bloom, et al. J. Power Sources 124 (2) (2003) 538.
cciv. Y. Itou, Y. Ukyo, J. Power Sources 146 (1) (2005) 39.
ccv. A.R. Armstrong, P.G. Bruce, Nature 381 (6582) (1996) 499.
ccvi. M. Gu, et al. ACS Nano 7 (1) (2012) 760.
ccvii. J. Tu, et al. Electrochim. Acta 51 (28) (2006) 6456.
ccviii. M. Wohlfahrt-Mehrens, et al. J. Power Sources 127 (1–2) (2004) 58.
ccix. S.R. Gowda, et al. Phys. Chem. Chem. Phys. 16 (15) (2014) 6898.
ccx. H. Zheng, et al. J. Power Sources 207 (2012) 134.
ccxi. D.P. Abraham, et al. Electrochem. Solid State Lett. 11 (12) (2008) A226.
ccxii. X. Han, et al. J. Power Sources 251 (2014) 38.
ccxiii. Y.I. Jang, et al. Electrochem. Solid State Lett. 1 (1) (1998) 13.
ccxiv. G. Ceder, S. Mishra, Electrochem. Solid State Lett. 2 (11) (1999) 550.
ccxv. E. Rossen, et al. Solid State Ionics 57 (3–4) (1992) 311.
ccxvi. K. Kang, et al. Science 311 (5763) (2006) 977.
ccxvii. N. Yabuuchi, T. Ohzuku, J. Power Sources 119–121 (2003) 171.
ccxviii. K.M. Shaju, P.G. Bruce, Adv. Mater. 18 (17) (2006) 2330.
ccxix. M.M. Thackeray, et al. J. Mater. Chem. 17 (30) (2007) 3112.
ccxx. S. Hy, et al. J. Am. Chem. Soc. 136 (3) (2013) 999.
ccxxi. Y.-K. Sun, et al. Nat. Mater. 8 (4) (2009) 320.
ccxxii. M.M. Thackeray, Prog. Solid State Chem. 25 (1) (1997) 1.
ccxxiii. M.M. Thackeray, et al. J. Power Sources 21 (1) (1987) 1.
ccxxiv. M.M. Thackeray, J. Am. Ceram. Soc. 82 (12) (1999) 3347.
ccxxv. D.K. Kim, et al. Nano Lett. 8 (11) (2008) 3948.
ccxxvi. F. Jiao, P.G. Bruce, Adv. Mater. 19 (5) (2007) 657.
ccxxvii. E. Hosono, et al. Nano Lett. 9 (3) (2009) 1045.
ccxxviii. H.-W. Lee, et al. Nano Lett. 10 (10) (2010) 3852.
ccxxix. Y.L. Ding, et al. Adv. Funct. Mater. 21 (2) (2011) 348.
ccxxx. Y.-K. Sun, et al. Electrochim. Acta 48 (5) (2003) 503.
ccxxxi. M.-J. Lee, et al. Nano Lett. (2014).
ccxxxii. T. Kakuda, et al. J. Power Sources 167 (2) (2007) 499.
ccxxxiii. B. Deng, et al. Electrochim. Acta 49 (11) (2004) 1823.
ccxxxiv. T. Numata, et al. J. Power Sources 97–98 (2001) 358.
ccxxxv. Z. Chen, K. Amine, J. Electrochem. Soc. 153 (2) (2006) A316.
ccxxxvi. B. Li, et al. J. Mater. Chem. A 1 (41) (2013) 12954.
ccxxxvii. F. Jiao, et al. Angew. Chem. 120 (50) (2008) 9857.
ccxxxviii. M.S. Islam, C.A. Fisher, Chem. Soc. Rev. 43 (1) (2014) 185.
ccxxxix. J. Cho, et al. Chem. Mater. 12 (12) (2000) 3788.
ccxl. M. Yoncheva, et al. J. Mater. Sci. 46 (22) (2011) 7082.
ccxli. A. Sobkowiak, et al. Chem. Mater. 25 (15) (2013) 3020.
ccxlii. F. Lin, et al. Nat. Commun. (2014) 5.
ccxliii. S.K. Martha, et al. J. Electrochem. Soc. 158 (10) (2011) A1115.
ccxliv. K.S. Nanjundaswamy, et al. Solid State Ionics 92 (1–2) (1996) 1.
ccxlv. M. Armand, et al., Method for synthesis of carbon-coated redox materials with controlled size, Google Patents US (2004).
ccxlvi. S.-Y. Chung, et al. Nat. Mater. 1 (2) (2002) 123.
ccxlvii. C. Delacourt, et al. Electrochem. Solid State Lett. 9 (7) (2006) A352.
ccxlviii. Y.J. Lee, et al. Science 324 (5930) (2009) 1051.
ccxlix. S.-i. Nishimura, et al. Nat. Mater. 7 (9) (2008) 707.
ccl. J. Kim, et al. Energy Environ. Sci. 6 (3) (2013) 830.
ccli. C. Delacourt, et al. J. Electrochem. Soc. 152 (5) (2005) A913.
cclii. S. Okada, et al. J. Power Sources 97 (2001) 430.

ccliii. J. Wolfenstine, J. Allen, J. Power Sources 136 (1) (2004) 150.
ccliv. H. Gwon, et al. Adv. Funct. Mater. 19 (20) (2009) 3285.
cclv. H. Huang, et al. Adv. Mater. 14 (21) (2002) 1525.
cclvi. N. Recham, et al. Nat. Mater. 9 (1) (2010) 68.
cclvii. T. Mueller, et al. Chem. Mater. 23 (17) (2011) 3854.
cclviii. J. Barker, et al. J. Electrochem. Soc. 150 (10) (2003) A1394.
cclix. C. Masquelier, L. Croguennec, Chem. Rev. 113 (8) (2013) 6552.
cclx. B. Sergio, P. Stefania, Nanotechnology for Sustainable Energy, vol. 1140, American Chemical Society, (2013), p. 67.
cclxi. F. Wang, et al. Nat. Commun. 3 (2012) 1201.
cclxii. F. Wang, et al. J. Am. Chem. Soc. 133 (46) (2011) 18828.
cclxiii. A.J. Gmitter, et al. J. Power Sources 217 (2012) 21.
cclxiv. F. Badway, et al. Chem. Mater. 19 (17) (2007) 4129.
cclxv. F. Wu, et al. Adv. Energy Mater. 4 (11) (2014).
cclxvi. M.Q. Zhao, et al. Nat. Commun. 5 (2014) 3410.
cclxvii. C. Luo, et al. ACS Nano 7 (9) (2013) 8003.
cclxviii. D.-W. Wang, et al. J. Mater. Chem. A 1 (33) (2013) 9382.
cclxix. Y.L. Wang, et al. Energy Environ. Sci. 4 (10) (2011) 3947.
cclxx. T. Li, et al. Electrochim. Acta 68 (2012) 202.
cclxxi. C. Li, et al. Adv. Energy Mater. 3 (1) (2013) 113.
cclxxii. Z. Zhang, et al. RSC Adv. 4 (30) (2014) 15489.
cclxxiii. F. Badway, et al. J. Electrochem. Soc. 150 (10) (2003) A1318.
cclxxiv. Y. Zheng, et al. Solid State Commun. 152 (17) (2012) 1703.
cclxxv. H.C. Yu, et al. Energy Environ. Sci. 7 (5) (2014) 1760.
cclxxvi. A.J. Gmitter, et al. J. Mater. Chem. 20 (20) (2010) 4149.
cclxxvii. X. Hua, et al. J. Phys. Chem. C (2014).
cclxxviii. P. Liu, et al. J. Phys. Chem. C 116 (10) (2012) 6467.
cclxxix. Z.-W. Fu, et al. J. Electrochem. Soc. 152 (2) (2005) E50.
cclxxx. Z. Wei-Jun, J. Power Sources (2011) 196.
cclxxxi. D.R. Lide, Handbook of Chemistry and Physics, CRC Press, Boca Raton, FL, 2005.
cclxxxii. S.W. Kim, et al. Adv. Mater. 22 (46) (2010) 5260.
cclxxxiii. R. Ma, et al. Nanoscale 5 (14) (2013) 6338.
cclxxxiv. Q. Chu, et al. Electrochim. Acta 111 (2013) 80.
cclxxxv. X. He, et al. J. Power Sources 190 (1) (2009) 154.
cclxxxvi. M. Ebner, et al. Science 342 (6159) (2013) 716.
cclxxxvii. W. Li, et al. Proc. Natl. Acad. Sci. U. S. A. 110 (18) (2013) 7148.
cclxxxviii. N. Jayaprakash, et al. Angew. Chem. 50 (26) (2011) 5904.
cclxxxix. Z. Wei Seh, et al. Nat. Commun. 4 (2013) 1331.
ccxc. Z.W. Seh, et al. Chem. Sci. 4 (9) (2013) 3673.
ccxci. Z.W. Seh, et al. Chem. Sci. (2013).
ccxcii. Z.W. Seh, et al. Energy Environ. Sci. (2013).
ccxciii. M. Nagao, et al. J. Mater. Chem. 22 (19) (2012) 10015.
ccxciv. Y. Fu, et al. J. Am. Chem. Soc. 135 (48) (2013) 18044.
ccxcv. K.P. Cai, et al. Nano Lett. 12 (12) (2012) 6474.
ccxcvi. G. Luo, et al. J. Renew. Sustain. Energy 4 (6) (2012) 063128.
ccxcvii. F. Wu, et al. J. Mater. Chem. A 2 (17) (2014) 6064.
ccxcviii. D. Aurbach, et al. J. Electrochem. Soc. 156 (8) (2009) A694.
ccxcix. Z. Lin, et al. Adv. Funct. Mater. 23 (8) (2013) 1064.
ccc. E. Peled, et al. J. Power Sources 26 (3–4) (1989) 269.
ccci. L. Suo, et al. Nat. Commun. 4 (2013) 1481.
cccii. J.T. Lee, et al. Adv. Mater. 25 (33) (2013) 4573.
ccciii. J. Hassoun, B. Scrosati, Adv. Mater. 22 (45) (2010) 5198.
ccciv. Z. Lin, et al. Angew. Chem. 125 (29) (2013) 7608.
cccv. Z. Lin, et al. ACS Nano 7 (3) (2013) 2829.
cccvi. C. Luo, et al. ACS Nano 7 (9) (2013) 8003.
cccvii. C.-P. Yang, et al. Angew. Chem. Int. Ed. 52 (32) (2013) 8363.
cccviii. D. Kundu, et al. J. Power Sources 236 (2013) 112.
cccix. Y.L. Wang, et al. Energy Environ. Sci. 4 (10) (2011) 3947.